HHS Public Access

Author manuscript

Nat Struct Mol Biol. Author manuscript; available in PMC 2023 February 01.

Published in final edited form as:

Nat Struct Mol Biol. 2022 August ; 29(8): 774–780. doi:10.1038/s41594-022-00807-6.

Mechanism of client selection by the protein quality control factor UBE2O

Matthew C.J. Yip[1,*], **Samantha F. Sedor**[1,*], **Sichen Shao**[1,†]

[1]Department of Cell Biology, Harvard Medical School, 240 Longwood Ave., Boston, MA 02115

Abstract

The E2/E3 enzyme UBE2O ubiquitylates diverse clients to mediate important processes, including targeting unassembled 'orphan' proteins for quality control and clearing ribosomes during erythropoiesis. How quality control factors such as UBE2O select clients based on heterogeneous features is largely unknown. Here, we show that UBE2O client selection is regulated by ubiquitin binding and a cofactor, NAP1L1. Attaching a single ubiquitin onto a client enhances UBE2O binding and multi-monoubiquitylation. UBE2O also repurposes the histone chaperone NAP1L1 as an adaptor to recruit a subset of clients. Cryo-EM structures of human UBE2O in complex with NAP1L1 reveal a malleable client recruitment interface which is autoinhibited by the intrinsically reactive UBC domain. Adding a ubiquitylated client identifies a distinct ubiquitin-binding SH3-like domain required for client selection. Our findings reveal how multivalency and a feed-forward mechanism drive the selection of protein quality control clients.

Protein degradation by the ubiquitin-proteasome system (UPS) is essential for maintaining protein homeostasis and shaping cellular proteomes[1]. This process requires the conjugation of ubiquitin onto client proteins through a cascade of ubiquitin activating (E1), ubiquitin conjugating (E2 or UBC), and ubiquitin ligase (E3) activities. While dozens of E2 enzymes and hundreds of E3 ligases are separately encoded in metazoans, UBE2O (also called E2-230K) is one of only two known hybrid E2/E3 enzymes that can directly engage clients (i.e. E3 activity) and conjugate ubiquitin onto clients (i.e. E2 activity)[2-6]. In addition, with reported functions in orphan protein quality control, proteome remodeling, and signaling regulation, UBE2O ubiquitylates a diverse set of clients ranging from unassembled ribosomal proteins to tumor suppressors[2,3,5-10]. Reflecting its fundamental role in mammalian physiology, UBE2O is required for erythropoiesis, but UBE2O amplification is also associated with poor prognoses in numerous cancers[3,7,9-11].

Although many UBE2O clients have juxtaposed basic and hydrophobic patches, these recognition elements are degenerate in sequence and occur in various contexts on proteins that range widely in size, structure, and binding partners[2,6,12]. It is unclear how such

†Correspondence: sichen_shao@hms.harvard.edu.
*These authors contributed equally

Author contributions

M.C.J.Y. identified UBE2O ubiquitin binding activity and collected and processed cryo-EM data. S.F.S. identified NAP1L1. M.C.J.Y. and S.S. built atomic models. S.S. supervised the project. M.C.J.Y, S.F.S, and S.S. wrote the paper.

Competing interests

The authors have no competing interests to declare.

heterogeneous client features trigger UBE2O engagement and ubiquitylation. By combining interaction assays, biochemical reconstitutions, and single-particle cryogenic electron microscopy (cryo-EM), we show that UBE2O leverages a previously unannotated ubiquitin binding site and the chaperone NAP1L1 as substrate adaptors to ubiquitylate different clients. Our findings reveal how a composite client-binding interface coupled with an affinity-mediated feed-forward mechanism drives the selection of diverse clients by UBE2O.

Results

UBE2O preferentially binds and modifies ubiquitylated clients

We made an unexpected insight into UBE2O client selection by assaying the interaction between UBE2O and the putative client interferon related developmental regulator 2 (IFRD2) (Fig. 1a). IFRD2 is a ribosome-inactivating protein which is stabilized in UBE2O knockout reticulocytes[3] and whose expression closely mirrors that of UBE2O during erythroid differentiation[13-16] (Extended Data Fig. 1a). Consistent with the assignment of IFRD2 as a UBE2O client, we selectively detected ubiquitylated IFRD2 in cells transiently expressing wildtype (WT) but not catalytically dead (CD) UBE2O in which the catalytic cysteine at position 1040 is mutated (Fig. 1a). IFRD2 pulldowns revealed a specific interaction with WT but not CD UBE2O, which was surprising because disrupting UBC activity should not affect the client binding site of UBE2O.

The specific interaction between IFRD2 and WT UBE2O was explained by reciprocal UBE2O pulldowns showing that WT UBE2O selectively enriches ubiquitylated IFRD2 and depletes unmodified IFRD2 (Fig. 1b). Fusing ubiquitin with a G76V mutation to prevent cleavage by deubiquitinases onto IFRD2 (referred to as Ub-IFRD2) (Extended Data Fig. 1b) was sufficient to introduce an interaction with both WT and CD UBE2O (Fig. 1b, **orange arrowheads**). This interaction was disrupted by mutating three residues (L8/I44/V70) in the ‘hydrophobic patch’ of ubiquitin [referred to as Ub(3A)-IFRD2] commonly recognized by ubiquitin-binding domains[17] (Fig. 1b). These data indicate that UBE2O has an unannotated ubiquitin-binding domain which selectively increases affinity for ubiquitylated clients.

In vitro ubiquitylation reactions revealed that UBE2O ubiquitylated Ub-IFRD2 more efficiently than unmodified IFRD2 or Ub(3A)-IFRD2 (Fig. 1c). Similar results were seen with a known orphan protein client of UBE2O, the large ribosomal subunit protein uL2[2], and ubiquitin-fused uL2 (Ub-uL2) (Extended Data Fig. 1c). We did not observe significant differences in client ubiquitylation when we performed ubiquitylation reactions with methylated ubiquitin incapable of forming polyubiquitin chains, or when we mutated all lysines in the ubiquitin portion of Ub-IFRD2 to arginines (Extended Data Fig. 1d,e). Thus, UBE2O does not specifically build polyubiquitin chains, consistent with previous reports that UBE2O primarily carries out multi-monoubiquitylation[2,3,5,6,18]. These findings reveal a feed-forward mechanism in which ubiquitin-linked clients have higher affinity for UBE2O and are preferentially subjected to further ubiquitylation.

NAP1L1 regulates UBE2O client selection

Analysis of different UBE2O clients revealed another unexpected observation in the recurring association of a protein identified by mass spectrometry as nucleosome assembly protein 1-like 1 (NAP1L1) (Extended Data Fig. 2a). NAP1L1 is a conserved homodimeric histone chaperone[19,20] which interacts with both WT and CD UBE2O (Extended Data Fig. 2b). We could also assemble UBE2O-NAP1L1 complexes *in vitro* and purify UBE2O-NAP1L1 complexes from cells (Fig. 2a; Extended Data Fig. 2c). Sequential affinity purifications suggested that NAP1L1 can form ternary complexes with UBE2O and an orphan ribosomal protein, and chemical crosslinking indicated that NAP1L1 directly interacts with a UBE2O client (Extended Data Fig. 2d,e). In all cases, we could not detect NAP1L1 ubiquitylation. These results suggest that NAP1L1 directly interacts with UBE2O clients and with UBE2O but is not targeted for ubiquitylation. Importantly, knocking out NAP1L1 abolished the interaction between uL2 and UBE2O (Fig. 2b, **compare lanes 1-3 and 7-9**). Re-expressing NAP1L1 (Extended Data Fig. 3a,b) or fusing ubiquitin onto uL2 (Ub-uL2) (Fig. 2b, **lanes 10-12**) restores interaction with UBE2O, while the strongest interaction with UBE2O was observed with Ub-uL2 in the presence of NAP1L1 (Fig. 2b, **lanes 4-6**). Thus, NAP1L1 and ubiquitin independently enhance UBE2O binding to uL2.

To determine if NAP1L1 independently interacts with UBE2O clients, we performed client pulldowns in UBE2O knockout cells to assay interactions with endogenous NAP1L1. This revealed an interaction between uL2 and NAP1L1 which was not affected by UBE2O expression (Fig. 2c, **lanes 1 and 2**). However, re-expressing UBE2O strongly enhanced the interaction between Ub-uL2 and NAP1L1 (Fig. 2c, **lanes 3 and 4**). In comparison, IFRD2 did not interact with NAP1L1 in any condition tested (Fig. 2c, **lanes 5-8**), and NAP1L1 depletion did not disrupt the interaction between IFRD2 and UBE2O (Extended Data Fig. 3c). Thus, NAP1L1 helps to select only a subset of UBE2O clients, and UBE2O client selection benefits from the combined avidities of possible interactions between NAP1L1 and UBE2O, between NAP1L1 and client, between UBE2O and client, and between UBE2O and ubiquitin attached to a client (Fig. 2d).

Out of five closely related human NAP1-like proteins (NAP1L1-NAP1L5), NAP1L1 and NAP1L4 are the most broadly expressed[20-22] (Supplementary Fig. 1). Knocking out NAP1L1 increased NAP1L4 interaction with UBE2O, indicating that UBE2O may be capable of exchanging substrate adaptors (Extended Data Fig. 3d). However, knocking out NAP1L4 did not affect the interaction between uL2 and UBE2O (Extended Data Fig. 3e), suggesting that NAP1L1 is the main adaptor for uL2 and that NAP1 paralogs may have non-redundant functions in complex with UBE2O.

Structure of UBE2O in complex with NAP1L1

To gain molecular-level insights into client selection by UBE2O and NAP1L1, we determined the structure of CD UBE2O in complex with NAP1L1 using single-particle cryogenic electron microscopy (cryo-EM) to an overall resolution of 3.3 Å (Fig. 3a-c; Extended Data Figs. 4, 5; Table 1; Supplementary Video 1). The UBE2O-NAP1L1 complex resembles an upside-down ‘J’. The NAP1L1 dimer forms the mostly horizontal bar of the ‘J’. In this orientation, we refer to the left and right subunits as NAP1L1-A and NAP1L1-B,

respectively. The three conserved regions (CR1, CR2, and CR3)[2,3,6] and the UBC domain of UBE2O are mostly resolved in the cryo-EM map and form the hook of the 'J' (Fig. 3a,b).

CR1 and CR2 form the straight edge of the hook with three SH3-like domains (SH3-A, SH3-B, and SH3-C) and two tandem SH3-like domains (tSH3-A and tSH3-B), while the UBC domain and a CR3 helix form the curved edge of the hook (Fig. 3a-c; Extended Data Fig. 5d-f). tSH3-A is the only domain which contains structural elements contributed by both CR1 and CR2 and scaffolds the other CR1-CR2 domains (Fig. 3a-c). tSH3-B extends from between α3 and β1 of tSH3-A to asymmetrically interact with NAP1L1, and SH3-B and SH-C pack on top of the two tSH3 domains (Fig. 3b,c). An interaction between SH3-B and the CR3 helix connects the two parts of the hook, while ~200 unresolved residues (711-927) between SH3-C and the UBC domain must reach across the width of the 'J' (Fig. 3c; Extended Data Fig. 6a).

We propose that clients engage the interior of the 'J', which would place them near the catalytic cysteine in the UBC domain of UBE2O (Fig. 3c; Extended Data Fig. 6b). This composite interface may be modulated by several flexible elements. First, a flexible β-hairpin loop of NAP1L1-B (β5-β6, residues 270-293) rich in basic residues juts upwards towards the UBC domain of UBE2O (Extended Data Fig. 6a; Supplementary Fig. 1). This loop would line the putative client binding cavity and may regulate client binding. Second, on both NAP1L1 subunits, 42 unresolved residues in the acidic C-terminal tail implicated in yeast NAP1 to bind ribosomal proteins[23] would extend towards the client binding interface (Fig. 3c). Finally, disordered and charged regions of UBE2O flanking CR1 and CR2 (Extended Data Fig. 5g), including the sequence which links CR2 and the UBC domain, may sample or reside in the interior of the 'J'. These flexible and charged elements in UBE2O and NAP1L1 may help engage proteins with heterogeneous basic and hydrophobic patches characteristic of UBE2O clients[2,3,6,12,24].

UBE2O binds NAP1L1 through electrostatic interactions

The interaction between UBE2O tSH3-B and NAP1L1 involves charged interfaces and buries over 1500 Å^2. Acidic residues in NAP1L1 that contribute to a composite UBE2O-binding groove include E345, E348, and D349 in a C-terminal loop of NAP1L1-A located on one side of the β4-β5 loop of UBE2O tSH3-B, and D243, D248, and E251 in the β3-β4 loop of NAP1L1-B on the other side (Fig. 4a). These elements contribute to a highly acidic platform which may interact with basic residues in UBE2O tSH3-B, including K289 and K291 in the β4-β5 loop, and R293 in β5. To validate this interaction, we reversed basic charges on UBE2O. Although mutating K289, K291, or R293 to aspartate individually had little effect on the interaction between UBE2O and NAP1L1, a double K289/291E mutant of UBE2O severely impaired NAP1L1 binding, and the triple mutant did not detectably bind NAP1L1 (Fig. 4b). Thus, electrostatics drives the interaction between UBE2O and NAP1L1.

The UBC domain autoinhibits client binding and is intrinsically active

During data processing, we observed a class of apo UBE2O which appears to adopt a different conformation than UBE2O in complex with NAP1L1 (Extended Data Fig. 4b). Although preferential orientation prevented accurate modeling of apo UBE2O (Extended

Data Fig. 6c), docking the UBE2O-NAP1L1 model into a map of apo UBE2O and comparing 2D class averages suggest that the UBC domain of apo UBE2O swings inward towards CR1-CR2 (Fig. 4c; Extended Data Fig. 6d). Supporting the idea that this region is dynamic, the local resolution of the UBC domain in the UBE2O-NAP1L1 map is lower than the rest of the complex (Extended Data Fig. 4c). In addition, unlike full-length UBE2O, UBE2O lacking the UBC domain can bind unmodified IFRD2 (Fig. 4d). These results suggest that the UBC domain autoinhibits client binding by UBE2O. NAP1L1 may relieve this autoinhibition by displacing the UBC domain based on the position of the NAP1L1-B β5-β6 hairpin loop (Extended Data Fig. 6a), introducing conformational changes that expose the client-binding interface, and directly recruiting clients (Fig. 2c).

Next, we analyzed the E2 activity of UBE2O. UBE2O is considered a 'class IV' E2 based on the presence of long N- and C-terminal extensions beyond the UBC domain. UBE2O and two other class IV E2s belong to a subfamily characterized by an insert with a conserved 'TWxG' motif in loop 7 of the UBC domain[25] (Supplementary Fig. 2). The other members of this family are BIRC6, the only other E3-independent E2 in the ubiquitin-proteasome system[26], and UBE2Z. The UBC domain of UBE2O adopts a canonical E2 fold with two additional helices (α5 and CR3/α6), also seen in BIRC6 and UBE2Z, that pack against α4 and the backside of the UBC domain[27] (Extended Data Fig. 7a). To isolate E2 activity, we physically separated the N-terminal portion of UBE2O (residues 1-887, referred to as UBE2O-N) from UBC-CR3 (residues 888-1292). UBE2O-N enhanced the ubiquitylation of a model client by UBC-CR3 *in vitro*[5] (Extended Data Fig. 7b), confirming the complementation of client binding and E2 activities. To specifically assay E2 activity, we performed single-turnover ubiquitin discharge assays by adding free lysine to pre-charged E2~Ub conjugates. As expected, experiments with the E3-dependent E2 UbcH5a showed a low rate of ubiquitin discharge which was enhanced by the E3 ligase RNF4[28] (Fig. 4e; Extended Data Fig. 7c). In contrast, isolated UBC-CR3 of UBE2O exhibited significant intrinsic ubiquitin discharge activity which was not affected by the addition of UBE2O-N. Thus, although the lysine reactivity of most E2 enzymes requires activation by an E3, the UBC domain of UBE2O exhibits intrinsic lysine reactivity that is not further activated by the client-binding portion of UBE2O.

UBE2O binds ubiquitin through a SH3-like domain

Finally, to explain how UBE2O preferentially engages ubiquitylated clients, we determined the cryo-EM structure of UBE2O-NAP1L1 in complex with Ub-uL2 to an overall resolution of 3.5 Å (Fig. 5a,b; Extended Data Fig. 8; Table 1; Supplementary Video 1). Classification of this dataset revealed heterogeneity in the relative positions and orientations of NAP1L1 and UBE2O domains around the client-binding interface (Extended Data Fig. 9a-c; Supplementary Video 2). Although we did not observe density for uL2, which may flexibly or heterogeneously bind the complex, all conformations of the complex contained a distinct density not seen in the UBE2O-NAP1L1 complex that clearly corresponds to ubiquitin (Fig. 5a,b; Extended Data Fig. 9d,e).

Ubiquitin binds the SH3-C domain of UBE2O (Fig. 5a,b; Supplementary Video 3), which places K48 (and other lysines) of the bound ubiquitin approximately 30 Å from the catalytic

cysteine in the UBC domain (Extended Data Fig. 9f). This position rules out the possibility that the ubiquitin is a substrate for polyubiquitin chain formation. A handful of SH3 domains (e.g. of Sla1) and the SH3-like CAP-Gly domains in the deubiquitinase CYLD also bind ubiquitin[29-31]. However, superposing these structures with ubiquitin-bound SH3-C revealed completely different binding interfaces (Extended Data Fig. 10a). On UBE2O, the L8/I44/V70 hydrophobic patch of the bound ubiquitin faces a hydrophobic patch centered on I660 and I662 at the end of β1 of SH3-C (Fig. 5c). Mutating I660 and I662 of UBE2O to alanines (referred to as I660/662A UBE2O) abolished ubiquitin-enhanced binding to IFRD2 (Fig. 5d; Extended Data Fig. 10b) and interaction with Ub-uL2 in the absence of NAP1L1 (Extended Data Fig. 10c). *In vitro* ubiquitylation assays revealed that I660/662A UBE2O did not proceed beyond mono-ubiquitylation and did not ubiquitylate ubiquitin-conjugated clients more efficiently than unmodified clients (Fig. 5e; Extended Data Fig. 10d). Autoubiquitylation of I660/662A UBE2O was not impaired, indicating selective disruption of activity towards ubiquitylated clients. These findings assign a previously unknown ubiquitin binding interface to an SH3-like domain which plays a key role in UBE2O client selection.

Discussion

Our findings reveal that UBE2O leverages multivalency and a feed-forward mechanism to select clients for ubiquitylation. We have identified a distinct ubiquitin-binding domain and NAP1L1 as substrate adaptors for UBE2O that function both independently and synergistically. Initial interactions with individual elements on UBE2O and/or NAP1L1 are probably weak, resulting in short residence times that would not permit client ubiquitylation. However, clients able to engage multiple sites on UBE2O alone or in complex with NAP1L1 would persist longer, favoring ubiquitylation. Ubiquitin conjugation would introduce another potential interaction with SH3-C of UBE2O to further increase avidity. Thus, UBE2O employs a malleable interface to capture substrates, which may facilitate the selection of diverse unassembled protein quality control clients with degenerate and heterogeneous recognition features[2,32]. Selecting clients based on multivalency contributed by composite elements also may prioritize the ubiquitylation of orphan proteins with multiple inappropriately exposed assembly interfaces. In addition, the possibility of exchanging substrate adaptors[12], including paralogs of NAP1L1, may provide a means to tune UBE2O function and clientele in different physiological contexts. Compounding affinities with varied interaction sites on quality control complexes may be a generalizable principle for the selection of diverse protein quality control clients.

Methods

Plasmids and antibodies

Initial constructs encoding UBE2O (a gift from the Hegde lab), Cmd1-DDX56 (a chimeric protein of yeast Cmd1 fused to residues 436-547 of DDX56; a gift from the Finley lab), and IFRD2 were as previously described[2,3,16]. The cDNA sequences for uL2 (MHS6278-202757330) and NAP1L1 (MHS6278-202826639) were purchased from Dharmacon. cDNA sequences for uL14 and uS3 were obtained from PlasmID. For

expression in mammalian cells, the open reading frames of IFRD2, UBE2O, uL2, uL14, and NAP1L1 were cloned into a pcDNA3.1 mammalian expression vector encoding an N-terminal FLAG, Strep, or HA tag. UBE2O-N (residues 1-887), ΔUBC UBE2O (lacking residues 944-1113), UBE2O CR1 (residues 1-450), and point mutants were generated using standard molecular biology techniques. Point mutations of cysteine at position 1040 to either serine or lysine to generate catalytically dead (CD) UBE2O were introduced by Phusion mutagenesis. No functional differences were observed between C1040S or C1040K UBE2O. Ubiquitin (G76V) was inserted into IFRD2 or uL2 vectors by Gibson assembly, and the Ub(3A) mutant was generated by Phusion mutagenesis. To purify ubiquitin-bound UBE2O-NAP1L1 for cryo-EM analysis, Ub-uL2 was inserted into the Strep-tagged UBE2O vector by Gibson assembly. FLAG-tagged NAP1L1 was subcloned into a pcDNA5/FRT/TO vector for stable cell line generation in Flp-In 293 T-REx cells, or into the pHAGE vector for lentiviral expression. Helper plasmids for lentiviral assembly were obtained from PlasmID. The plasmid to purify UbcH5a was a gift from the Finley lab. The plasmid to express Cys-ubiquitin was a gift from Zhejian Ji and the Rapoport lab. The plasmid to express murine E1 enzyme was a gift from Ellen Goodall and the Harper lab.

Guide RNAs targeting UBE2O (ATGTGCCGGACCACATCTCG), NAP1L1 (CTAACCTTTCAGCCTGCCTA), and NAP1L4 (TCCGTGAGCGGATAGTCCCG) were designed using ChopChop v3[33] and inserted into pX459[34] by ligation of annealed primers into the BbsI-digested backbone. For bacterial expression, untagged NAP1L1, FLAG-tagged NAP1L1, IFRD2, and Ub-IFRD2 variants were inserted into a pGEX vector containing an N-terminal GST tag, and UBC-CR3 (residues 888-1292) and Cmd1-DDX56 were inserted into a pK27 vector containing an N-terminal His-SUMO tag using standard molecular biology techniques. For PURE reactions[35], uL2 and ubiquitin-fused variants were inserted into the PURExpress plasmid (NEB) containing a T7 promoter. Point mutations were made using Phusion mutagenesis. For *in vitro* translation in rabbit reticulocyte lysate, uL14 and uS3 were inserted into an pSP64-based vector[36].

HRP-conjugated anti-FLAG M2 (Sigma A8592, 1:10,000), anti-NAP1L1 (Proteintech 14898-1-AP, 1:500 or Abcam ab178687, 1:10,000), anti-NAP1L4 (Proteintech 16018-1-AP, 1:4,000), anti-UBE2O (Bethyl A301-873A, 1:5000), and HRP-conjugated StrepTactin (Bio-rad 1610381, 1:5000) were purchased. Polyclonal anti-HA serum was a gift from Ramanujan Hegde and used at 1:5000 for immunoblotting.

Cell culture and cell line generation

HEK293T and Flp-In 293 T-REx cells were cultured in Dulbecco's Modified Eagle's Medium (DMEM) with 10% fetal calf serum (FCS) at 37°C and 5% CO_2. Expi293F cells were cultured in Expi293 media (Gibco A1435101) at 37°C and 8% CO_2 and shaking at 120 rpm.

To generate knockout cell lines, 0.5-1 μg of pX459 containing individual guide RNAs were transfected into HEK293T or Flp-In 293 T-REx cells in a 6-well plate using TransIT-293 (Mirus) according to the manufacturer's instructions. After 24 h, the cells were placed under 2 μg mL^{-1} puromycin (Gibco A11138) selection for 48 h. Single clones were isolated and knockouts were confirmed by immunoblotting and genotyping. To generate NAP1L1 rescue

cell lines, UBE2O/NAP1L1 double knockout Flp-In 293 T-REx cells were co-transfected with the pcDNA5/FRT/TO plasmid containing FLAG-tagged NAP1L1 and pOG44 encoding for the Flp recombinase in a 1:1 ratio using TransIT-293 according to the manufacturer's instructions. Two days after transfection, cells were placed under selection and maintained with 10 μg mL^{-1} blasticidin S HCl (Gibco A11139) and 100 μg mL^{-1} hygromycin B (Gibco 10687). NAP1L1 expression was induced with 100 ng mL^{-1} doxycycline 24 h prior to transfection.

To generate a polyclonal population of Expi293F cells stably expressing FLAG-tagged NAP1L1, pHAGE-NAP1L1 was transfected into HEK293T cells together with helper plasmids (pHDM-VSVG, pHDM-MGPM2, pHDM-tat1B and pRC-CMV-rev1B) using TransIT-293 in a 6 cm plate according to the manufacturer's instructions and the media was changed after 24 h. 48 h after transfection, the media containing lentivirus was collected and syringe filtered. 500 μL lentivirus and 10 μg mL^{-1} polybrene was added to ~60 million Expi293F cells in a total volume of 20 mL. 48 h after infection, the Expi293F cells were placed under selection and maintained with 2 μg mL^{-1} puromycin for 4-5 generations.

UBE2O and client pulldowns

In general, 1 μg each of plasmids encoding Strep-tagged UBE2O and FLAG-tagged client, HA-tagged client, or FLAG-tagged NAP1L1 were co-transfected into HEK293T or Flp-In 293 T-REx cells using TransIT-293 in a 6-well plate according to the manufacturer's instructions. 16-24 h after transfection, the cells were harvested in cold PBS, lysed in 50 μL IP buffer [50 mM HEPES pH 7.5, 100 mM KOAc, 2.5 $Mg(OAc)_2$, 1% Triton X-100] with 1 mM dithiothreitol (DTT), 1x cOmplete protease inhibitor cocktail (PIC; Roche 1187358), and BioLock (IBA 2-0205; for StrepTactin pulldowns) for 10 min on ice, and clarified by centrifugation at 21,130 x g for 10 min at 4°C. For experiments where lysate concentrations needed to be normalized (Fig. 2b; Extended Data Fig. 3b,e and 10c), the cells were lysed in the same buffer with 1% digitonin instead of 1% Triton X-100 and normalized based on A_{280} readings prior to pulldowns. For pulldowns, lysates were diluted in 500 μL IP buffer and incubated with anti-FLAG M2 agarose resin (Sigma A2220) or StrepTactin HP resin (Cytiva 28-9355) for 1 h at 4°C. The beads were washed three times with IP buffer and eluted with protein sample buffer (for FLAG pulldowns) or IP buffer containing 5-10 mM desthiobiotin (for StrepTactin pulldowns) (Sigma D1411), which was then added to protein sample buffer. To analyze UBE2O association with NAP1L4 (Extended Data Fig. 3d), cells were harvested 3 days after transfection with Strep-tagged UBE2O and pulldowns were washed with 50 mM Tris pH 8, 250 mM NaCl, 1.5 mM $MgCl_2$, 1 mM DTT instead of IP buffer. For sequential FLAG and StrepTactin pulldowns (Extended Data Fig. 2d), one 10 cm dish was co-transfected with 3.5 μg Strep-tagged CD UBE2O and 3.5 μg FLAG-tagged-uL14 with TransIT-293 and lysed in IP buffer. The lysate was diluted and incubated with StrepTactin HP resin for 1 h at 4°C, washed three times with IP buffer, and eluted with IP buffer containing 10 mM desthiobiotin. The eluate was then incubated with anti-FLAG M2 resin for 1 h at 4°C, washed 3 times, and eluted in protein sample buffer.

Protein purifications and complex validations

GST-tagged IFRD2 and its ubiquitin variants (Fig. 1c) were expressed in Rosetta2 cells, which were transformed, grown in TB at 37°C under the appropriate antibiotic selection to an OD_{600} of 0.6 – 0.8, and induced overnight with 0.2 mM isopropyl β-d-1-thiogalactopyranoside (IPTG) at 18°C. The cells were harvested, resuspended in lysis buffer (1x PBS, 350 mM NaCl, 1 mM DTT) with 1x PIC, lysed by sonication, and clarified by centrifugation at 34,541x g. The supernatant was passed over glutathione Sepharose 4B (Cytiva 170756), washed with at least 10 column volumes of lysis buffer, and eluted in three column volumes of 50 mM Tris pH 8 with 25 mM reduced glutathione. The eluate was buffer exchanged into PBS using PD-10 columns and incubated with 1:1000 (v/v) GST-tagged 3C protease for 2 h on ice then 15 min at 25°C. The 3C protease and GST tag were then subtracted using glutathione Sepharose 4B. GST-NAP1L1 and GST-FLAG-NAP1L1 (Extended Data Fig. 2e) were expressed in BL21(DE3) cells, which were transformed, grown in LB, and purified under the same conditions as IFRD2 except the cells were lysed and washed in 1X PBS with 1 mM DTT and 1x PIC. The eluate was dialyzed into PSB [50 mM HEPES pH 7.5, 100 mM KOAc, 2.5 $Mg(OAc)_2$] with 10% glycerol and 1 mM DTT for 4 h, incubated with 1:1000 (v/v) GST-tagged 3C protease while dialyzing overnight at 4°C, then cleaved and subtracted as above. GST-tagged UbcH5a was expressed in BL21(DE3) cells, which were transformed, grown in TB, induced, and purified in the same way as GST-NAP1L1, except that the eluate was dialyzed into PSB with 1 mM DTT for 4 h, incubated with 1:1000 (v/v) GST-tagged 3C protease while dialyzing overnight at 4°C, before subtraction.

His-SUMO-tagged UBC-CR3, His-SUMO-tagged Cmd1-DDX56, and His-tagged murine E1 were expressed in Rosetta2 cells, which were transformed, grown in TB at 37°C under the appropriate antibiotic selection to an OD_{600} of 0.6 – 0.8, and induced overnight with 0.2 mM IPTG at 18°C. The cells were harvested, resuspended in lysis buffer containing 20 mM imidazole and 1x PIC, lysed by sonication, and clarified by centrifugation at 34,541x g. The supernatant was passed over NiNTA resin (Qiagen 30210), washed with at least 10 column volumes of lysis buffer with 20 mM imidazole, and eluted in three column volumes of lysis buffer with 300 mM imidazole. The UBC-CR3 and Cmd1-DDX56 eluates were dialyzed into PSB with 1 mM DTT for 4 h, incubated with 1:1000 (v/v) His-tagged Ulp1 (SUMO protease) while dialyzing overnight into PSB containing 1 mM DTT. The His-SUMO tag and His-tagged SUMO protease were then subtracted using NiNTA resin. The murine E1 eluate was dialyzed into PSB containing 1 mM DTT overnight at 4°C, then applied to a Superdex200 10/300 GL pre-equilibrated in PSB with 1 mM DTT. His-SUMO-tagged Cys-ubiquitin was expressed in BL21 (DE3) cells, which were transformed, grown in LB at 37°C under the appropriate antibiotic selection to an OD_{600} of 0.6 – 0.8, induced overnight with 0.2 mM IPTG at 18°C, and purified as described for UBC-CR3 and Cmd1-DDX56. For labeling, the cleaved and subtracted eluate was applied to a Superdex75 10/300 GL column pre-equilibrated with PSB lacking DTT. 600 μM of Cy5-maleimide (Abcam 146489) was added to 200 μM of Cys-ubiquitin and incubated overnight at 4°C in the dark. Unreacted dye was quenched with 5 mM DTT and removed with dye-removal columns (Thermo Scientific 22858) followed by size exclusion chromatography on a Superdex75 10/300 GL pre-equilibrated in PSB containing 1 mM DTT.

Strep-tagged UBE2O, UBE2O mutants, UBE2O-N, and NAP1L1 were purified from Expi293F cells seeded at 2.5 million cells mL^{-1}. 24 h later, the cells were diluted to 3 million cells mL^{-1} and 1 μg mL^{-1} of the construct was transfected with 5 μg mL^{-1} polyethyleneimine (PEI-25K; Polysciences 23966). 3 mM sodium valproate and 0.45% glucose were added to the cells 24 h after transfection. 48 h later, Expi293F cells were harvested, washed once in cold PBS, lysed in IP buffer with 1 mM DTT, 1x PIC, and BioLock for 10 min on ice, and clarified by centrifugation at 21,130 x g for 10 min at 4°C. The supernatant was incubated with StrepTactin HP resin for 1 h at 4°C, washed three times with IP buffer with 1 mM DTT and three times with wash buffer (IP buffer lacking Triton X-100 and with 1 mM DTT) before elution with 3 column volumes of wash buffer with 5 mM desthiobiotin. For size exclusion chromatography (Fig. 2a), NAP1L1 or WT UBE2O and NAP1L1 (at a 2:1 ratio of UBE2O to NAP1L1 dimer) were diluted in PSB with 1 mM DTT, incubated 15 min on ice, and applied to a pre-equilibrated Superose 6 10/300 GL column. The elution was collected in 0.2 mL fractions.

To purify UBE2O-NAP1L1 complexes with and without Ub-uL2 for structural analysis, 1 μg mL^{-1} of plasmids encoding Strep-tagged Ub-uL2-UBE2O or UBE2O was transfected into Expi293F cells constitutively expressing FLAG-tagged NAP1L1. 24 h before transfection, 100 mL of Expi293F cells were seeded at 2.5 million cells mL^{-1}. For transfection, the cells were diluted to 3 million cells mL^{-1} and transfected using 5 μg mL^{-1} PEI-25K. 3 mM sodium valproate and 0.45% glucose were added 24 h after transfection. 48 h later, cells were harvested, washed once in cold PBS, lysed in IP buffer with 1 mM DTT and 1x PIC for 10 min on ice, and clarified by centrifugation at 15,000 x g for 10 min at 4°C. The supernatant was incubated with 3 mL of anti-FLAG M2 resin, washed three times with IP buffer with 1 mM DTT and three times with wash buffer, before elution with 3 column volumes of wash buffer with 0.15 mg mL^{-1} 3xFLAG peptide (Sigma). The eluate was then incubated with 300 μL of packed StrepTactin HP resin for 1 h at 4°C, washed three times with wash buffer with 0.3 mM CHAPS, before elution with 3 column volumes of wash buffer with 0.3 mM CHAPS and 5 mM desthiobiotin. The eluate was concentrated to 500 μL and separated on a Superose 6 10/300 GL column pre-equilibrated in wash buffer with 0.3 mM CHAPS. The UBE2O-NAP1L1 complexes shown in Extended Data Fig. 2c were purified using the same approach, except that FLAG-tagged NAP1L1 was co-transfected with Strep-tagged-UBE2O in Expi293F cells at 1 μg mL^{-1} each, CHAPS was not used, and the purification was completed after elution with desthiobiotin.

In vitro ubiquitylation and E2-ubiquitin discharge assays

2 μM recombinant IFRD2 or its ubiquitin-fused variants were incubated at 37°C with 500 nM UBE2O in the presence of 10 μM ubiquitin (Bio-Techne U-100H), 75 nM E1 (Bio-Techne E-306), and an energy regeneration system (ERS) containing 1 mM ATP, 1 mM GTP, 12 mM creatine phosphate and 20 μg mL^{-1} creatine kinase. At the indicated time points, samples were withdrawn and quenched with protein sample buffer. uL2 and its ubiquitin variants were synthesized in the PURE system (NEB E6800)[35] with ^{35}S-methionine using 10 ng μL^{-1} plasmid according to manufacturer's instructions for 2 h at 37°C. Ubiquitylation reactions contained 1:1 (v/v) PURE translation reaction, 500 nM

UBE2O, 10 μM ubiquitin, 75 nM E1, and ERS, and incubated at 37°C. At the indicated time points, samples were withdrawn and quenched with protein sample buffer.

For E2-ubiquitin discharge assays, 12 μM of UBC-CR3 or UbcH5a was incubated with 500 nM homemade mouse E1 and 50 μM Cy5-labeled ubiquitin in buffer containing 25 mM HEPES pH 7.5, 100 mM KOAc, 1 mM $MgCl_2$ and 5 mM ATP for 5 min at room temperature. The charging reaction was quenched with 1:10 (v/v) 0.3 M EDTA. The E2~Ub mixture was then diluted 5-fold into discharging buffer containing 25 mM HEPES pH 7.5, 100 mM KOAc and 37.5 mM lysine in the presence or absence of 400 nM RNF4 (Bio-Techne E2-210) or UBE2O-N and incubated at room temperature. Aliquots of the reactions were added to sample buffer containing or lacking 200 mM DTT at the indicated time points.

In vitro translation, crosslinking, and affinity purifications

For affinity purifications for protein identification (Extended Data Fig. 2a) and chemical crosslinking (Extended Data Fig. 2e), a rabbit reticulocyte lysate-based (RRL) system was used to translate *in vitro* transcription products encoding the protein of interest[36]. Translation reactions contained either cold methionine (for affinity purifications) or ^{35}S-methionine and were incubated for 30 min at 32°C. For crosslinking reactions, radiolabeled uL14 was synthesized in RRL with 1 μM recombinant untagged or FLAG-tagged NAP1L1. The reactions were diluted 10-fold in PSB, crosslinked with 250 μM BMH (Thermo Scientific #22330) for 1 h on ice, quenched with 25 mM DTT, and denatured in 1% SDS at 95°C for 5 min. 1 mL of IP buffer and anti-FLAG M2 resin were added to the reaction, which was incubated with rotation at 4°C for 1 h, washed three times, and eluted in protein sample buffer. For affinity purifications, translation reactions of FLAG-tagged uL14 or FLAG-tagged uS3 were spun in a TLA120.1 rotor (Beckman Coulter) at 435,400 x g for 30 min to pellet ribosomes. The supernatant was incubated with anti-FLAG M2 resin for 1 h at 4°C, washed six times, and eluted with 0.2 mg mL^{-1} 3xFLAG peptide. The eluate was precipitated with trichloroacetic acid, washed with acetone, dried, and resuspended in protein sample buffer. Prominent interactors, identified by SYPRO Ruby (Invitrogen S12000) staining of an SDS-PAGE gel, were excised and sent for mass spectrometry analysis.

Statistics and reproducibility

Generally, all biochemical results shown are representative of at least 2 independent replicates, as indicated in figure legends. The main finding in Extended Data Fig. 1d is validated through an orthogonal assay in Extended Data Fig. 1e. The main finding in Extended Data Fig. 2a is validated through orthogonal assays in Fig. 2a and Extended Data Fig. 2b-e. The main finding in Extended Data Fig. 3a is orthogonally validated in Fig. 2b,c and Extended Data Fig. 3b,c,e.

Cryo-EM sample preparation and data collection

For UBE2O-NAP1L1 complexes, 1 mg mL^{-1} of purified UBE2O-NAP1L1 complexes without or with Ub-uL2 was crosslinked with 250 μM BS3 (Thermo Fisher Scientific #21580) for 15 min on ice and quenched with 2.5 mM Tris pH 7.5. 3 μL of crosslinked

sample at 0.8 mg mL^{-1} was applied to glow-discharged 0.6/1 UltrAuFoil 300 mesh grids (Quantifoil) and frozen in liquid ethane using a Vitrobot Mark IV (ThermoFisher Scientific) set at 4°C and 100% humidity with a 30 sec wait time, 3 sec blot time and +8 blot force. For apo UBE2O, 3 μL of purified UBE2O at 0.5 mg mL^{-1} applied to glow-discharged 1.2/1.3 UltrAuFoil 300 mesh grids (Quantifoil) and frozen in liquid ethane using a Vitrobot Mark IV set at 4°C and 100% humidity with a 30 sec wait time, 3 sec blot time and +8 blot force. Two data collections were performed on PEGylated apo UBE2O. Briefly, 151 μM of MS(PEG)12 methyl-PEG-NHS-Ester reagent (Thermo Scientific #22685) was added to 0.7 mg mL^{-1} of apo UBE2O and incubated for 2 h on ice. The sample was then diluted to 0.35 mg mL^{-1} with 50 mM HEPES pH 7.5, 100 mM KOAc, 5 mM $MgOAc_2$, 1 mM DTT before freezing on UltrAuFoil R1.2/1.3 300 mesh grids as above. Alternatively, the sample was diluted with 50 mM HEPES pH 7.5, 100 mM KOAc, 5 mM $MgOAc_2$, 1 mM DTT and 0.002% NP-40, before freezing on R1.2/1.3 300 mesh Cu grids.

All datasets were collected using a Titan Krios (ThermoFisher Scientific) operating at 300 kV and equipped with a BioQuantum K3 imaging filter with a 20 eV slit width and a K3 summit direct electron detector (Gatan) in counting mode at a nominal magnification of 105,000x corresponding to a calibrated pixel size of 0.825 Å. Semi-automated data collection was performed with SerialEM. For the UBE2O + NAP1L1 dataset, a 3.116 sec exposure was fractionated into 52 frames and resulted in a total exposure of 57.4 electrons per $Å^2$. The defocus targets were −1.4 to −2.5. For the Ub-uL2-UBE2O + NAP1L1 dataset, a 1.501 sec exposure was fractionated into 55 frames and resulted in a total exposure of 59.6 electrons per $Å^2$. The defocus targets were −1.4 to −2.5. For the first apo UBE2O dataset, a 2.497 sec exposure was fractionated into 50 frames and resulted in a total exposure of 55.2 electrons per $Å^2$. The defocus targets were −1.5 to −2.5. For the PEGylated apo UBE2O dataset, a 1.6 sec exposure was fractionated into 49 frames and resulted in a total exposure of 54.7 electrons per $Å^2$. The defocus targets were −1.6 to −2.5. For the PEGylated apo UBE2O dataset collected with a stage tilt of 35°, a 1.3 sec exposure was fractionated into 50 frames and resulted in a total exposure of 51.094 electrons per $Å^2$. The defocus targets were −1.9 to −2.9.

Image processing

Data processing for UBE2O-NAP1L1 complexes was performed in cryoSPARC v3.3.1[37] (Extended Data Figs. 4, 8). After patch-based motion correction and CTF estimation, micrographs with severe contamination or poor CTF fits were removed. 7,796 (UBE2O-NAP1L1) or 7,765 (Ub-uL2-UBE2O-NAP1L1) micrographs were subjected to automated particle picking using templates generated from blob-based picking. The particles were extracted with a box size of 340 and downsampled to a box size of 170 for initial classification steps. After 2D classification, heterogeneous refinement was performed using multiple reference volumes generated by *ab initio* reconstruction. Particles in the best classes were subjected to non-uniform 3D refinement followed by another round of heterogenous refinement. Afterwards, particles were unbinned and subjected to non-uniform 3D refinement, global and local CTF refinement, and local motion correction. An additional round of 2D classification was applied to the Ub-uL2-UBE2O-NAP1L1 dataset. The final

particle set (447,881 particles for UBE2O-NAP1L1; 201,743 particles for Ub-uL2-UBE2O-NAP1L1) was subjected to a final round of non-uniform 3D refinement.

In addition, 3,677,176 particle coordinates (after 2D classification in cryoSPARC) in the Ub-uL2-UBE2O-NAP1L1 were imported into RELION v3.1[38] and extracted from micrographs that were subjected to CTF estimation and motion correction in RELION with a box size of 340. Following multiple rounds of 2D and 3D classification, particles in five classes were individually subjected to 3D refinement, CTF refinement and Bayesian polishing. The polished particles were used for 3D refinement and multibody refinement with masks around Ub-UBE2O and the NAP1L1. Masks around Ub-UBE2O in each of the five maps were also used to generate re-centered subtracted particle stacks that were individually subjected to 2D classification. Selected particles resulting from the best class averages were combined for a final round of 3D refinement to generate a map focused on Ub-UBE2O (Extended Data Fig. 9d,e).

Data processing for apo UBE2O was initially performed in cryoSPARC. Following patch-based motion correction and CTF estimation, micrographs with severe contamination or poor CTF fits were removed. 5,676 (no treatment), 4,855 (PEGylated), or 4,692 (tilted) micrographs were subjected to automated particle picking using templates generated from blob-based picking. The particles were extracted with a box size of 240 and downsampled to a box size of 60 for initial classification steps. After 2D classification, the particle coordinates of 1,026,147 (no treatment), 1,026,645 (PEGylated), or 1,319,787 (tilted) particles were imported into RELION v3.1 and extracted from micrographs that were subjected to CTF estimation and motion correction in RELION with a box size of 240 and downsampled to a box size of 60. Following a round of 2D and 3D classification, a total of 708,305 particles were un-binned and used for 3D auto-refinement. Afterwards, focused classification with signal subtraction was performed using a mask around the entire UBE2O density. A final particle set of 89,302 particles were subjected to 3D refinement, CTF refinement, and Bayesian polishing, followed by a final round of 3D refinement.

Model building and analysis

Half maps were post-processed using DeepEMhancer for interpretation and visualization[39]. Alphafold2 models of human UBE2O (Q9C0C9) and NAP1L1 (P55209)[40] were used as initial models that were fitted as rigid bodies into the cryo-EM map of the UBE2O-NAP1L1 complex in Chimera v1.15[41], followed by removal of unresolved residues in Coot v0.9[42]. UBC-CR3 (residues 928 to the C terminus) was separated from UBE2O-N, fitted as a rigid body in Chimera, followed by one round of Phenix real space refine v1.19[43] with only rigid body fitting enabled. The interaction between tSH3-B of UBE2O and NAP1L1-A was refined using a model generated by Alphafold-Multimer[44] using residues 220-300 of UBE2O and residues 340-355 of NAP1L1. After manual adjustments in Coot, multiple rounds of Phenix real space refine were performed with the experimental maps, with manual model inspection and adjustments in Coot and in ChimeraX v1.3[45] with ISOLDE v1.0[46] in between. Although the presence of NAP1L1 increased particle orientations of UBE2O-NAP1L1 compared to datasets of apo UBE2O, some preferential orientation was

still observed and affected β-strand continuity in UBE2O, limiting the estimated model resolution to 4.1 Å.

ColabFold[47] was used to generate initial models for ubiquitin bound to UBE2O (residues 55-89; 117-392; 479-878; 895-1147; 1230-1292), excluding flexible inter-CR segments of UBE2O. Of the five models generated, the second ranked model placed ubiquitin in the position corresponding to the extra density in the cryo-EM maps of UBE2O-NAP1L1 bound to ubiquitin. This model was aligned to the UBE2O-NAP1L1 model (RMSD of 2.642), resulting in good alignment of the SH3-C domains. The coordinates of ubiquitin were then combined with the UBE2O-NAP1L1 model and used to generate the model of the ubiquitin-bound UBE2O-NAP1L1 complex in Phenix, Coot, and ChimeraX as described above. Model validations were performed with MolProbity[48] and EMRinger[49] in Phenix. Figure panels were made with ChimeraX and Pymol[50]. Multiple sequence alignments (Supplementary Figs. 1, 2) were performed using mTM-align[51] or ClustalW[52,53] and visualized using ESPript 3.0[54]. UBE2O sequence conservation (Extended Data Fig. 5d-f) was analyzed using the ConSurf server[55] with multiple sequence alignments of a manually curated list of UBE2O homologs from amphibians, reptiles, fish, birds and mammals. Charge values (Extended Data Fig. 5g) were calculated using EMBOSS[56]. Data processing was supported by software packages installed and configured by SBGrid[57].

Extended Data

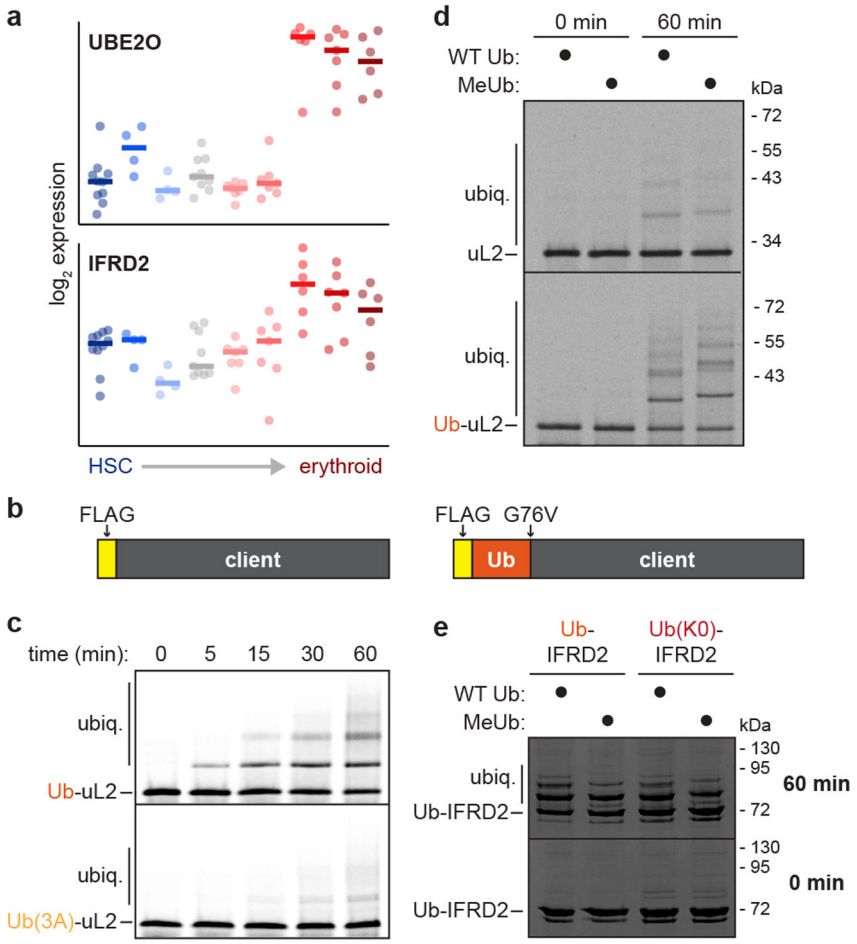

Extended Data Fig. 1 |. UBE2O has a ubiquitin-binding domain.

a, Expression (log_2) values of UBE2O or IFRD2 in human hematopoietic cells at different stages of differentiation from hematopoietic stem cells (HSC) through the erythroid lineage[13,14]. Data (left to right) are from HSC (CD133+ CD34dim), HSC (CD38− CD34+), common myeloid progenitor (CMP) cells, megakaryocyte-erythroid progenitor (MEP) cells, and the following erythroid cell types: CD34+ CD71+ GlyA−, CD34− CD71+ GlyA−, CD34− CD71+ GlyA+, CD34− CD71lo GlyA+, CD34− CD71− GlyA+. **b,** Scheme of IFRD2 and ubiquitin-fused IFRD2 (Ub-IFRD2) variants analyzed in Fig. 1. **c,** SDS-PAGE and phosphorimaging of *in vitro* ubiquitylation timecourses, representative of 3 replicates, of radiolabeled uL2 fused to wildtype ubiquitin (Ub-uL2) or to ubiquitin with a mutated hydrophobic patch [Ub(3A)-uL2], which were synthesized in the PURE translation system and then incubated with 500 nM UBE2O, 75 nM E1, 10 μM ubiquitin, and an energy regenerating system. Note: ubiquitylation of Ub-uL2 is more efficient than that of Ub(3A)-uL2. **d,** Autoradiography of *in vitro* ubiquitylation reactions of uL2 (top) and Ub-uL2 (bottom) as in **c**, with wildtype ubiquitin (WT Ub) or methylated ubiquitin (MeUb) incapable of polyubiquitin chain formation at the indicated timepoints. **e,** Coomassie staining of *in vitro* ubiquitylation reactions as in Fig. 1c of IFRD2 conjugated either to

wildtype ubiquitin (Ub-IFRD2) or to ubiquitin in which all lysines are mutated to arginines [Ub(K0)-IFRD2] with WT Ub or MeUb. Note: the degree of client ubiquitylation in reactions shown in **d** and **e** does not change substantially with Ub(K0) or MeUb.

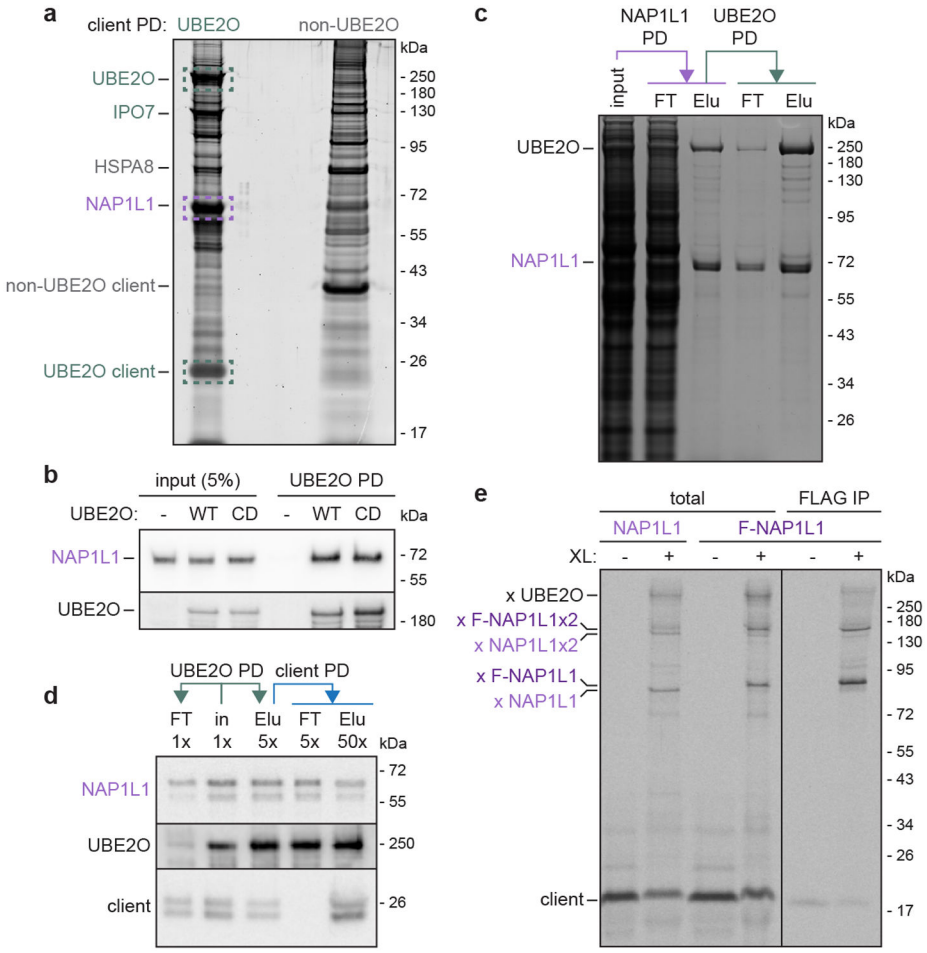

Extended Data Fig. 2 |. NAP1L1 interacts with UBE2O and UBE2O clients.

a, SDS-PAGE and SYPRO Ruby staining of pulldowns (PD) of a FLAG-tagged UBE2O client (uL14) or a FLAG-tagged non-UBE2O client (uS3) synthesized in a mammalian *in vitro* translation system. Labels indicate abundant bands which were excised and identified by mass spectrometry. Teal dotted boxes, UBE2O and UBE2O client. Purple dotted box indicates stoichiometric recovery of NAP1L1 with the UBE2O client but not the non-UBE2O client. **b,** UBE2O knockout Flp-In 293 T-REx cells co-expressing FLAG-tagged NAP1L1 without or with wildtype (WT) or catalytically dead (CD) Strep-tagged UBE2O were lysed (input), subjected to UBE2O PD, and analyzed by SDS-PAGE and immunoblotting, representative of >3 replicates. Note: NAP1L1 is not ubiquitylated and interacts equally well with WT and CD UBE2O. **c,** SDS-PAGE and Coomassie staining of sequential PDs of FLAG-tagged NAP1L1 and Strep-tagged UBE2O showing stoichiometric complex purification, representative of 2 replicates. FT, flow-through; Elu, elution. **d,** Cells co-expressing CD Strep-tagged UBE2O and a FLAG-tagged UBE2O client (uL14) were lysed and subjected to sequential UBE2O and client PDs. Input (in), FT, and

Elu samples at the indicated relative concentrations were analyzed by SDS-PAGE and immunoblotting, representative of 2 replicates, suggesting recovery of ternary complexes of UBE2O, NAP1L1, and uL14,. **e,** The radiolabeled UBE2O client uL14 was synthesized *in vitro* with either 1 μM untagged or FLAG-tagged NAP1L1 (F-NAP1L1), subjected to chemical crosslinking with 250 μM BMH as indicated, and analyzed directly (total) or after denaturing anti-FLAG immunoprecipitations (IP) by SDS-PAGE and autoradiography, representative of 2 replicates. Client crosslinks (x target) to UBE2O, NAP1L1, F-NAP1L1, and NAP1L1 or F-NAP1L1 dimers (x2) are indicated.

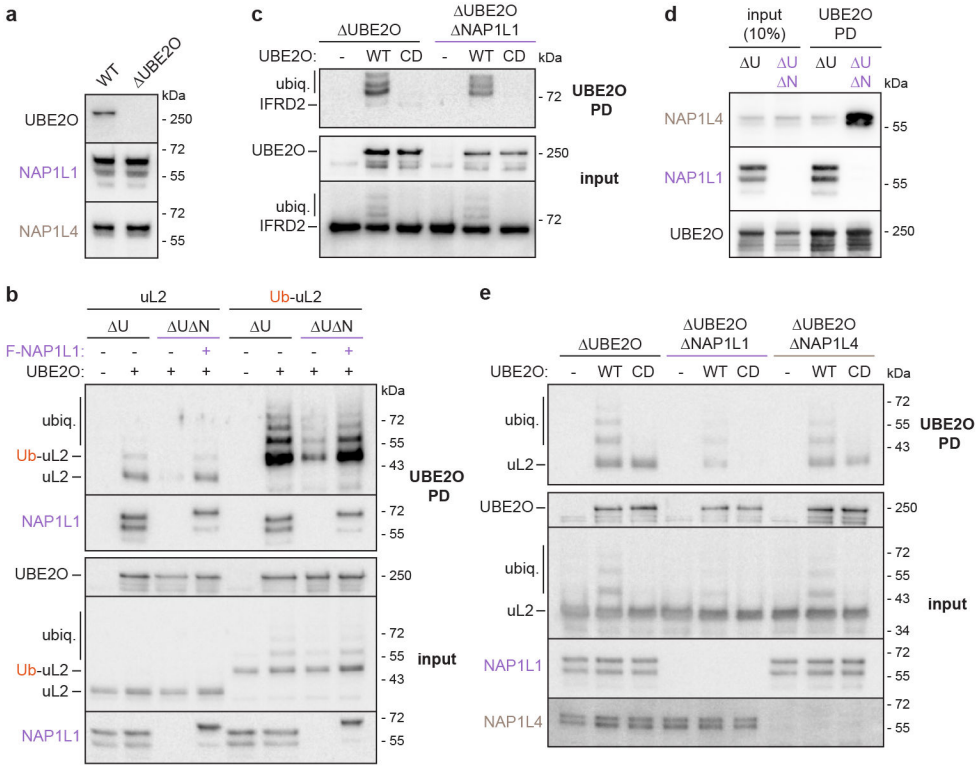

Extended Data Fig. 3 |. NAP1L1 recruits a subset of UBE2O clients.

a, Immunoblotting for UBE2O and NAP1 paralogs in wildtype (WT) or UBE2O knockout (ΔUBE2O) Flp-In 293 T-Rex cells. **b,** Pulldown (PD) of WT Strep-tagged UBE2O co-expressed with HA-tagged uL2 or Ub-uL2 in UBE2O knockout (ΔU) or UBE2O/NAP1L1 double knockout (ΔUΔN) Flp-In 293 T-Rex cells without or with induced re-expression of FLAG-tagged NAP1L1 (F-NAP1L1) incorporated into the Flp-In locus. F-NAP1L1 successfully rescues the interaction between uL2 and UBE2O which is impaired by knocking out NAP1L1, representative of 3 replicates. **c,** PD of WT or catalytically dead (CD) UBE2O co-expressed with FLAG-tagged IFRD2 in ΔUBE2O or ΔUBE2O ΔNAP1L1 Flp-In 293 T-Rex cells, showing that knocking out NAP1L1 does not strongly impair the interaction between IFRD2 and UBE2O, representative of 2 replicates. **d,** UBE2O purifications from ΔU or ΔUΔN cells showing NAP1L1 and NAP1L4 association. **e,** PD of WT or CD UBE2O co-expressed with FLAG-tagged uL2 in ΔUBE2O, ΔUBE2O ΔNAP1L1, or UBE2O/NAP1L4 double knockout (ΔUBE2O ΔNAP1L4) Flp-In 293 T-Rex

cells. Note: knocking out NAP1L1 but not NAP1L4 impairs uL2 association with UBE2O, representative of 3 replicates.

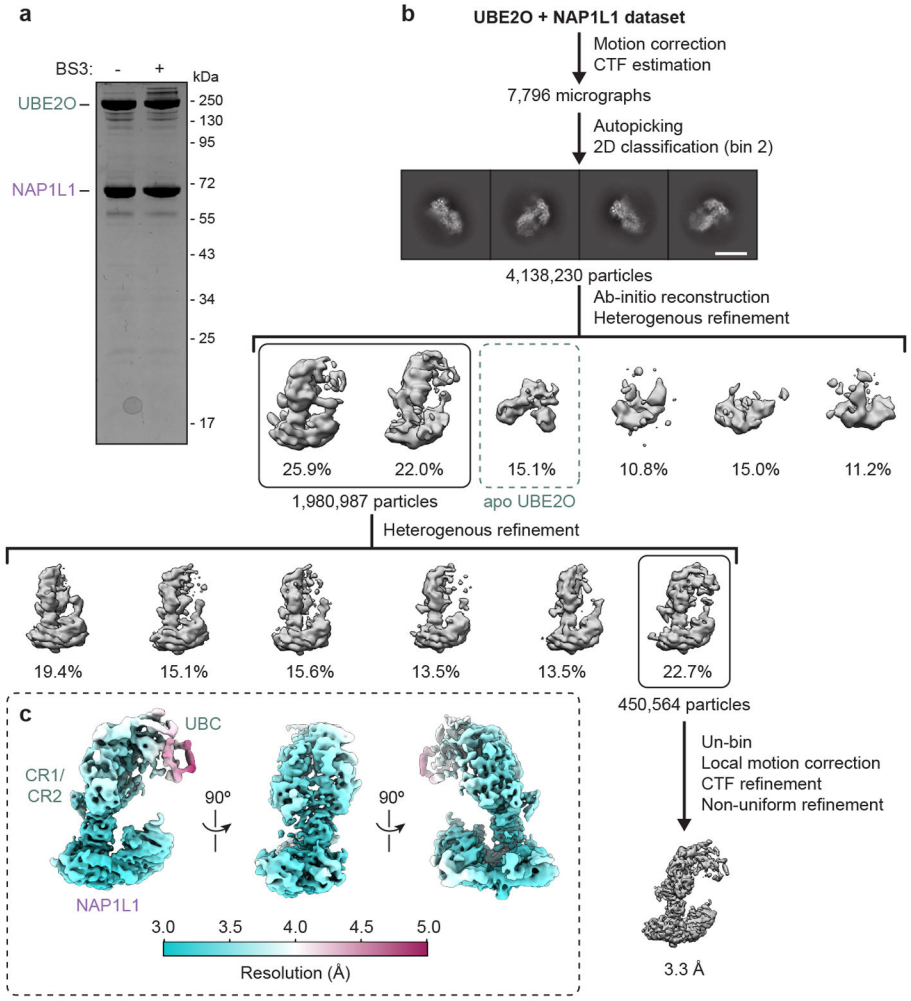

Extended Data Fig. 4 |. Cryo-EM data processing of UBE2O in complex with NAP1L1.
a, SDS-PAGE and Coomassie staining of purified UBE2O-NAP1L1 complex without and with crosslinking with 250 μM BS3 used for cryo-EM analysis, representative of 2 independent preparations. **b,** Summary of processing strategy for the UBE2O + NAP1L1 dataset. Teal dotted box denotes class of apo UBE2O. Scale bar, 10 nm. **c,** Cryo-EM map of UBE2O-NAP1L1 colored by local resolution.

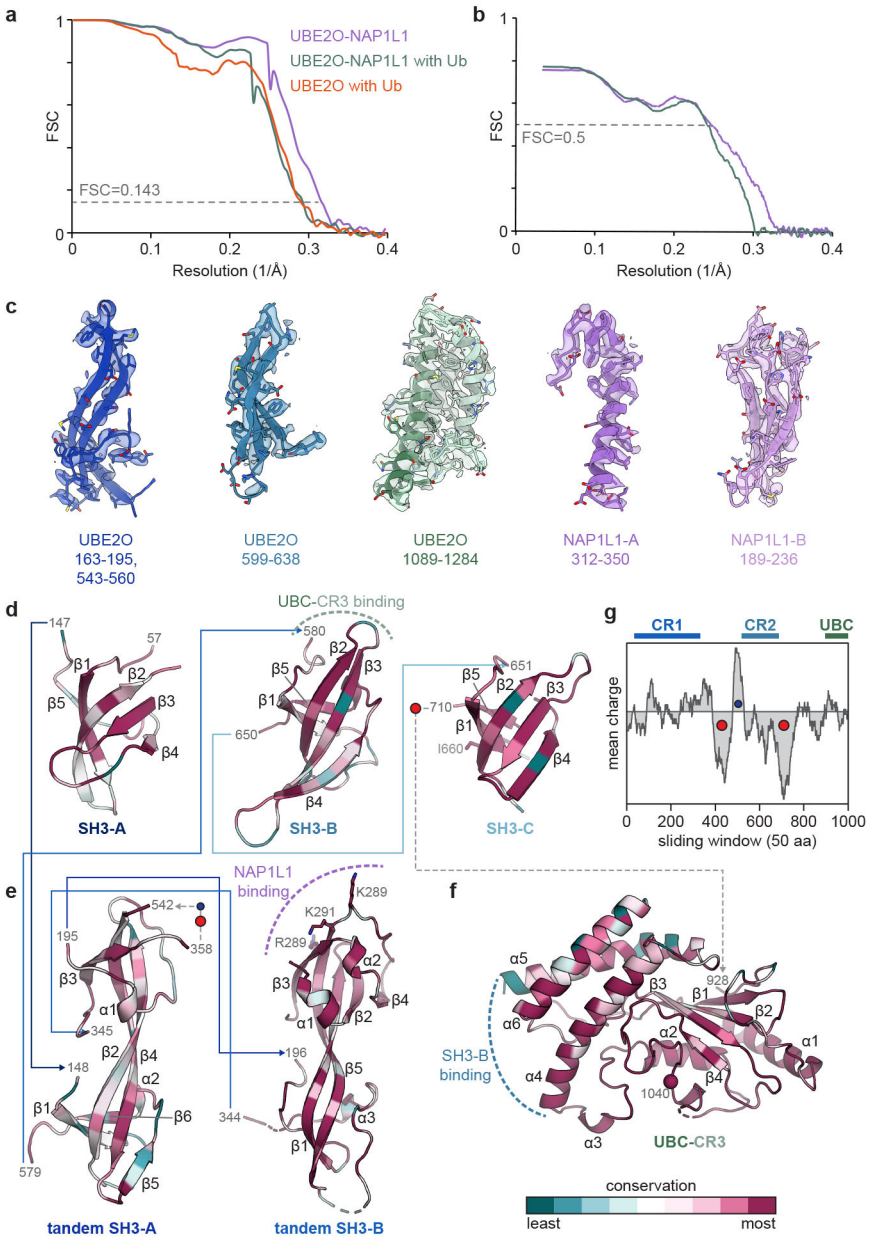

Extended Data Fig. 5 |. Cryo-EM maps and models.

a, Fourier shell correlation (FSC) coefficient vs. resolution ($Å^{-1}$) curves of the indicated maps. Resolution was estimated at FSC=0.143 (gray dotted line). **b,** Model vs. map FSC curves for structures as in **a. c,** Segmented EM map densities of the sharpened UBE2O-NAP1L1 map contoured at 8.6σ with corresponding atomic model. **d-f,** Secondary structure designations of the **d,** SH3-like domains, **e,** tandem SH3 domains, and **f,** UBC-CR3 of UBE2O colored by sequence conservation. Position of the catalytic cysteine is shown as a sphere. Connectivity between domains is indicated by lines with arrowheads and residue numbering. Dotted lines and labeled residues indicate interfaces involved in intra- and inter-molecular interactions. **g,** Net charge (calculated as +1 for K/R, +0.5 for H, −1 for D/E) over sliding windows of 50 amino acids across the UBE2O sequence. Positions of CR1,

CR2, and the beginning of UBC are indicated above. Red and blue circles indicate acidic and basic stretches, respectively.

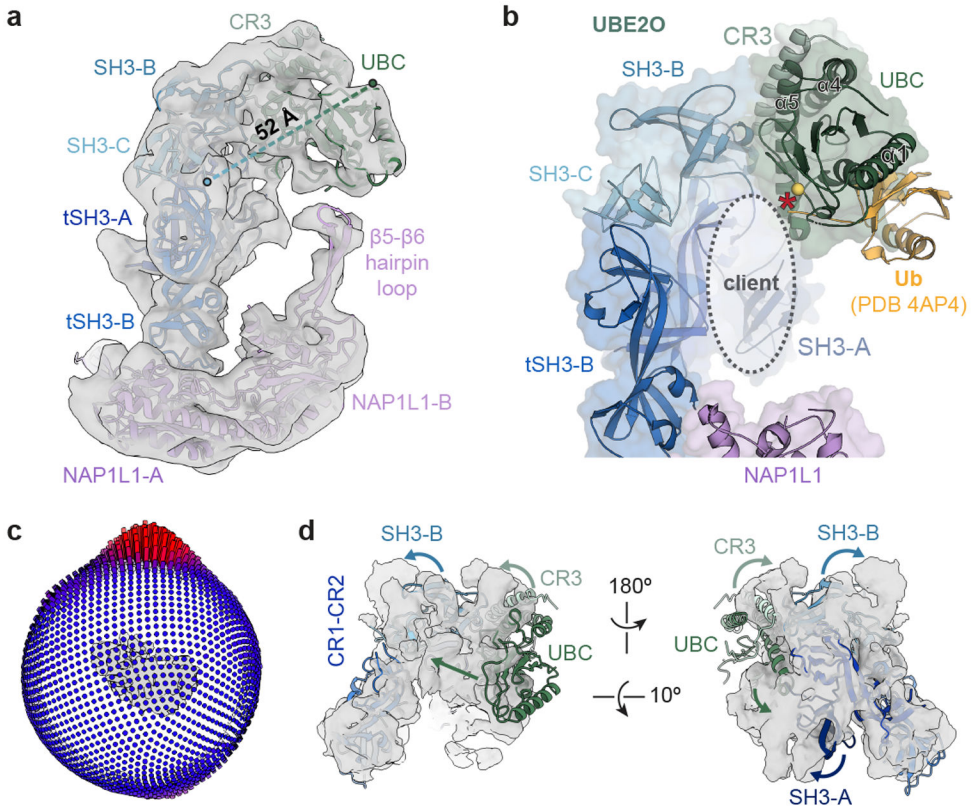

Extended Data Fig. 6 |. Contributions to UBE2O client binding.

a, Model of UBE2O-NAP1L1 docked into a downsampled and unsharpened cryo-EM map contoured at 4.9σ showing the position of the β5-β6 hairpin loop of NAP1L1-B and the linear distance (dotted line) between the C-terminal end of SH3-C and the N-terminal end of the UBC domain on UBE2O, which are connected by residues 711-927. These features may influence client engagement. **b,** Position of UBC-charged ubiquitin (Ub, light orange) in the UBE2O-NAP1L1 complex relative to the putative client binding cavity, based on superposition of the UBE2O UBC domain with ubiquitin-charged UbcH5a (PDB 4AP4). Yellow sphere, position of C1040. Red asterisk denotes active site for client ubiquitylation. **c,** Angular distribution of a cryo-EM map of apo UBE2O. Preferential orientation was not significantly improved despite combining three datasets of unmodified apo UBE2O and of PEGylated apo UBE2O without and with a stage tilt of 35°. **d,** Rigid body docking of the model of UBE2O in the UBE2O-NAP1L1 complex (Fig. 3c) into a cryo-EM map of apo UBE2O. Arrows indicate putative movements of the indicated domains to account for conformational differences.

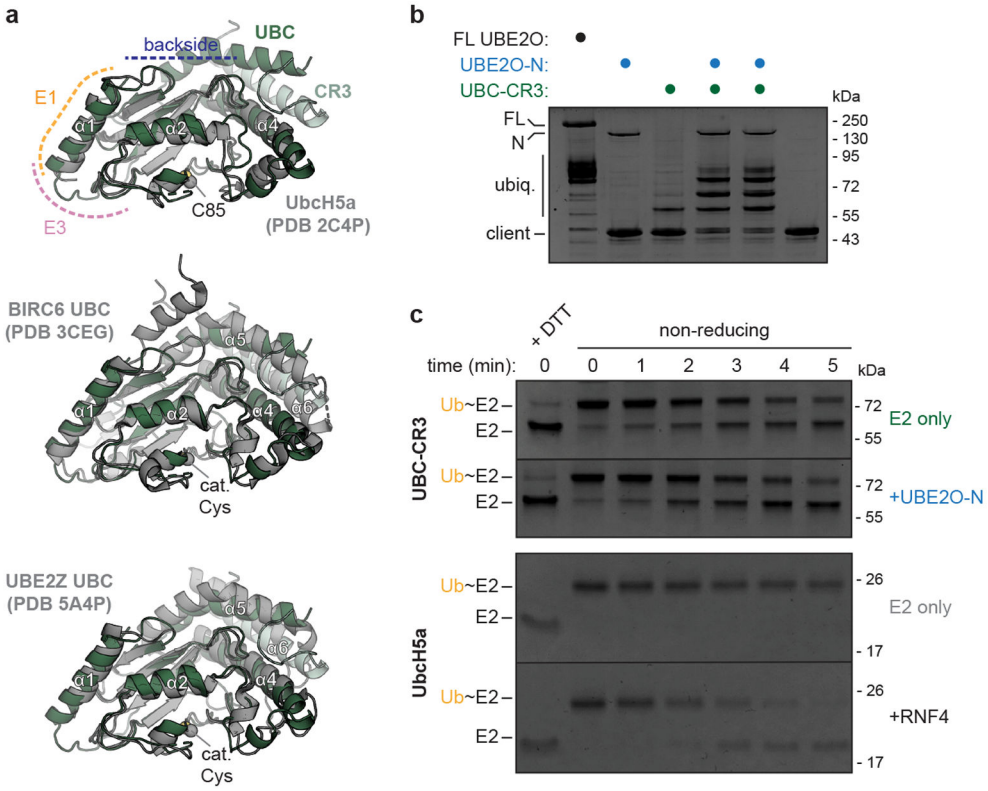

Extended Data Fig. 7 | Analysis of UBE2O E2 activity.

a, Superposition of UBC-CR3 of UBE2O (green) with the UBC domain (gray) of UbcH5a (PDB 2C4P, top), BIRC6 (PDB 3CEG, middle), or UBE2Z (PDB 5A4P, bottom). The E1 binding site (orange), the canonical RING E3 binding site (yellow), and the backside of the UBC domain (blue) are indicated relative to UbcH5a (top). Catalytic cysteines are shown as spheres. Note the additional helices (α5 and α6) present in UBC-CR3 of UBE2O and the UBC domains of BIRC6 and UBE2Z. **b,** *In vitro* ubiquitylation assays of a recombinant UBE2O client (Cmd1-DDX56)[3] with full-length (FL) UBE2O, the CR1 and CR2 regions of UBE2O (UBE2O-N), and/or UBC-CR3 of UBE2O as indicated. The non-endogenous Cmd1-DDX56 client was analyzed due to its efficient ubiquitylation. Note: effective ubiquitylation is achieved with FL UBE2O or with both UBC-CR3 and UBEO-N, but not with either domain individually, representative of 2 replicates. **c,** Ubiquitin discharging assays from UBE2O UBC-CR3 (top) or UbcH5a (bottom) onto free lysine without or with a corresponding E3 activity (UBE2O-N or RNF4, respectively), representative of 3 independent experiments quantified in Fig. 4e. Ub~E2, ubiquitin-charged E2.

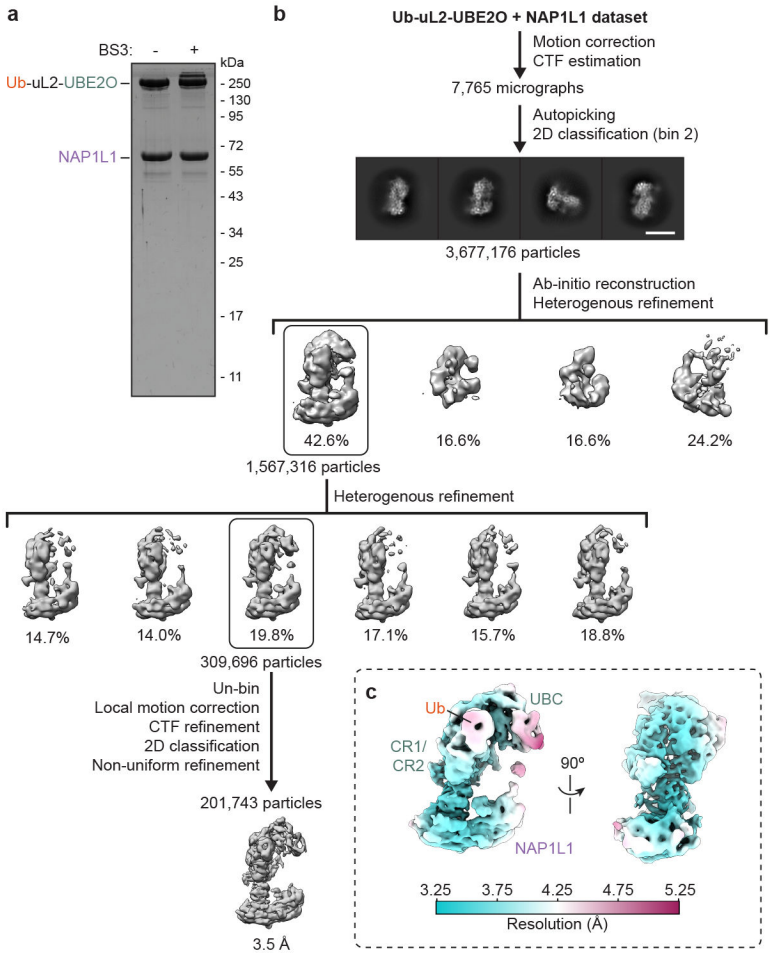

Extended Data Fig. 8 |. Cryo-EM data processing of UBE2O-NAP1L1 bound to Ub-uL2.
a, SDS-PAGE and Coomassie staining of purified Ub-uL2-UBE2O-NAP1L1 complex without and with crosslinking with 250 μM BS3 used for cryo-EM analysis, representative of 2 independent preparations. Note: Ub-uL2 is fused to UBE2O by a long linker but remains associated with the complex if this linker is cleaved after purification. **b,** Summary of processing strategy for the Ub-uL2-UBE2O + NAP1L1 dataset. Scale bar, 10 nm. **c,** Cryo-EM map of UBE2O-NAP1L1 bound to Ub-uL2 colored by local resolution.

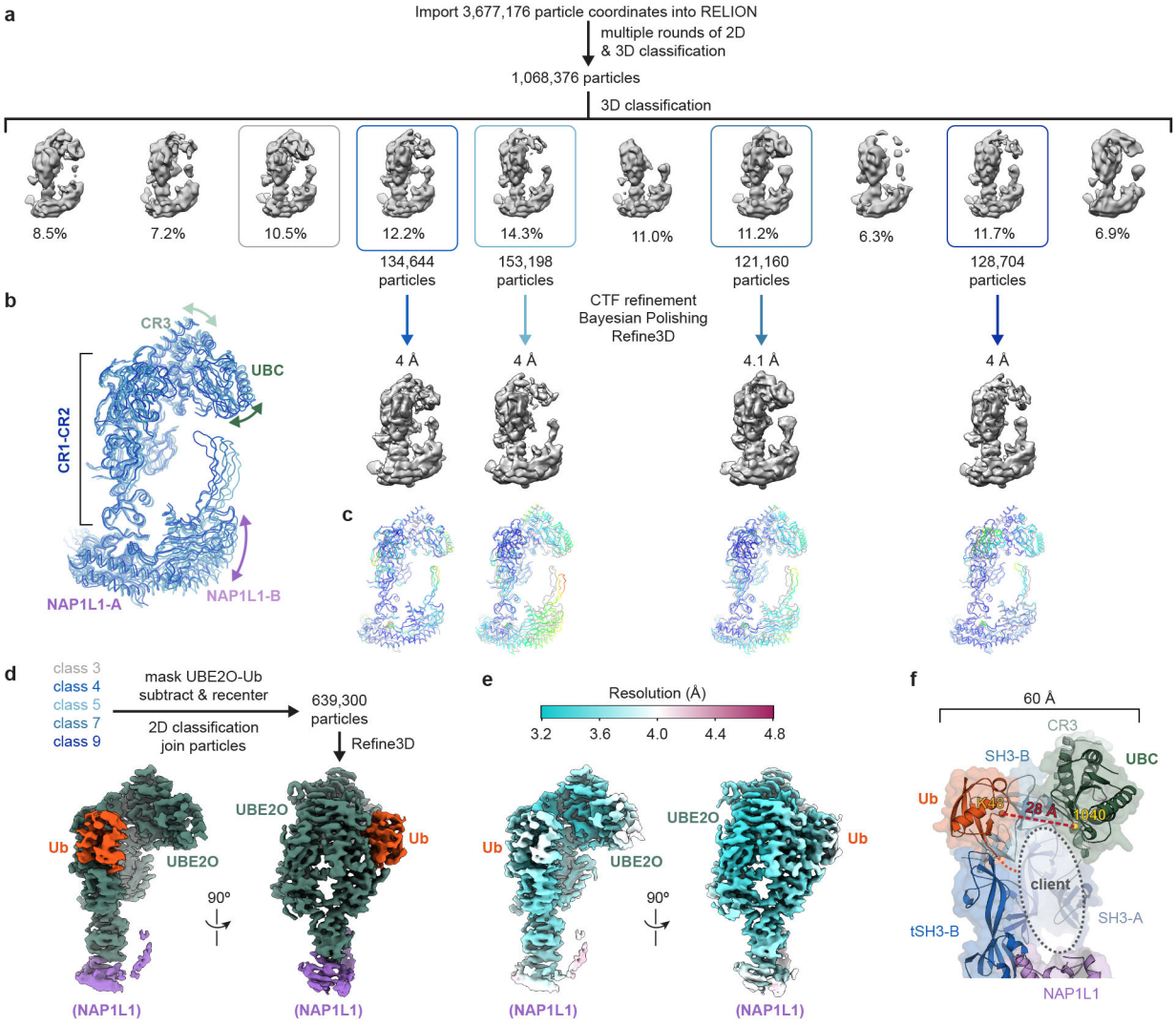

Extended Data Fig. 9 |. Analysis of UBE2O-NAP1L1 with Ub-uL2.

a, Summary of processing strategy to examine conformational heterogeneity of UBE2O-NAP1L1 bound to ubiquitin. **b,** Superposition of models in which individual UBE2O and NAP1L1 domains were fitted to cryo-EM maps of the indicated classes (blue boxes) showing conformational heterogeneity in the relative positions and orientations of NAP1L1-B, UBC, and CR3 around the putative client binding interface. **c,** Models as in **b**, fitted to the indicated cryo-EM maps and superposed with the consensus model of the Ub-UBE2O-NAP1L1 complex (gray; Fig. 5b) colored by RMSD (blue – lowest, red – highest, normalized to each model). **d,** Processing strategy to generate subtracted particles of ubiquitin-bound UBE2O for focused refinement. **e,** Cryo-EM map resulting from focused refinement of ubiquitin-bound UBE2O as in **d**, colored by local resolution. **f,** Position of ubiquitin (orange) bound to SH3-C of UBE2O. Lysine at position 48 (K48) of ubiquitin is shown together with the distance (red) to the catalytic cysteine at position 1040 (yellow) of UBE2O. The C-terminal end of ubiquitin, which is modeled up to residue 73 is indicated by the orange dotted line leading to the putative client binding cavity.

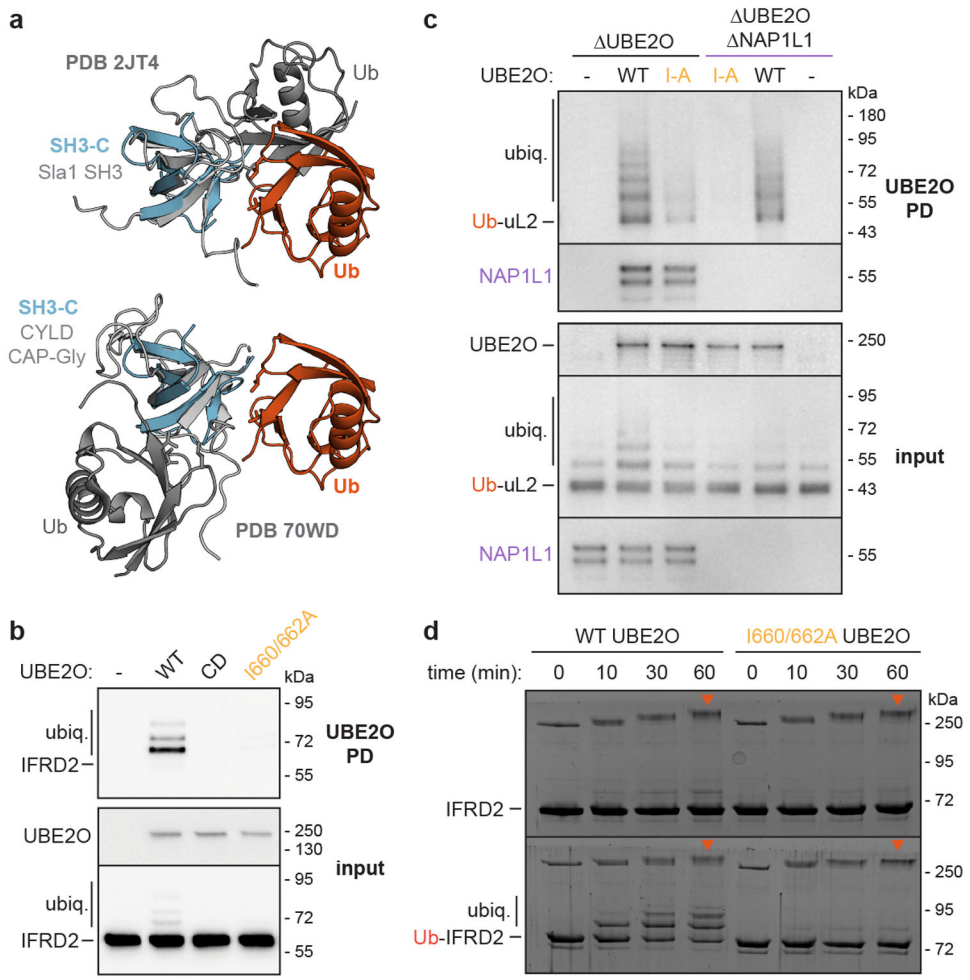

Extended Data Fig. 10 |. SH3-C of UBE2O binds ubiquitin.

a, Superposition of ubiquitin (Ub; orange) bound to SH3-C of UBE2O (light blue) with the SH3 domain of Sla1 (top; PDB 2JT4) or the CAP-Gly SH3-like domain of CYLD (bottom; PDB 70WD) (light gray) bound to ubiquitin (dark gray). Note: although the SH3 and SH3-like domains are well-aligned, they bind ubiquitin through different interfaces. **b,** Pulldown (PD) of wildtype (WT), catalytically dead (CD), or I660A/I662A Strep-tagged UBE2O co-expressed with FLAG-tagged IFRD2, representative of 2 replicates. ubiq., ubiquitylated client. **c,** PD of WT or I660A/I662 (I-A) Strep-tagged UBE2O co-expressed with FLAG-tagged ubiquitin-fused uL2 (Ub-uL2) in UBE2O knockout (ΔUBE2O) or UBE2O/NAP1L1 double knockout (ΔUBE2O ΔNAP1L1) cells, representative of 2 replicates. Note: I-A UBE2O loses ubiquitin-enhanced client binding activity. **d,** *In vitro* ubiquitylation timecourses of IFRD2 or ubiquitin-fused IFRD2 (Ub-IFRD2) with WT or I660A/I662A UBE2O, representative of 2 replicates. Orange arrowheads, autoubiquitylated UBE2O.

Supplementary Material

Refer to Web version on PubMed Central for supplementary material.

Acknowledgements

Cryo-EM data collection and screening were performed at the Harvard Center for Cryo-EM (HC2EM) and the Molecular Electron Microscopy Suite (MEMS) at Harvard Medical School. Data processing was supported by SBGrid. Mass spectrometry analysis was performed at the Taplin Mass Spectrometry Facility. The authors thank Xudong Wu and Ellen Goodall for experimental advice; Alan Brown, Dan Finley, Tom Rapoport, Wade Harper, and Geoff Nelson for critical reading; and Suzanne Elsasser, Miguel Prado, and Shao lab members for useful discussions. This work was supported by NIH DP2GM137415, a Packard Fellowship, and the Vallee Foundation (S.S.), American Heart Association predoctoral fellowship 287375208 (M.C.J.Y), and NIH F31HL157976 (S.F.S.).

Data Availability

EM maps and models are available under accession numbers EMD-26612, EMD-26614, EMD-26615, PDB 7UN3, and PDB 7UN6. All other data are available within the article and its Extended Data and Supplementary Information. Source data are provided with this paper. Correspondence and requests for materials should be directed to S.S.

References

1. Ubiquitin Signaling in Health and Disease [special issue]. Cell Death & Differentiation 28, (2021).
2. Yanagitani K, Juszkiewicz S & Hegde RS UBE2O is a quality control factor for orphans of multiprotein complexes. Science 357, 472–475 (2017). [PubMed: 28774922]
3. Nguyen AT et al. UBE2O remodels the proteome during terminal erythroid differentiation. Science 357, eaan0218 (2017). [PubMed: 28774900]
4. Berleth ES & Pickart CM Mechanism of Ubiquitin Conjugating Enzyme E2-230K: Catalysis Involving a Thiol Relay? Biochemistry 35, 1664–1671 (1996). [PubMed: 8634298]
5. Zhang X et al. Fine-tuning BMP7 signalling in adipogenesis by UBE2O/E2-230K-mediated monoubiquitination of SMAD6. EMBO J 32, 996–1007 (2013). [PubMed: 23455153]
6. Mashtalir N et al. Autodeubiquitination Protects the Tumor Suppressor BAP1 from Cytoplasmic Sequestration Mediated by the Atypical Ubiquitin Ligase UBE2O. Mol Cell 54, 392–406 (2014). [PubMed: 24703950]
7. Ullah K, Zubia E, Narayan M, Yang J & Xu G Diverse roles of the E2/E3 hybrid enzyme UBE2O in the regulation of protein ubiquitination, cellular functions, and disease onset. FEBS J 286, 2018–2034 (2019). [PubMed: 30468556]
8. Chen S et al. Ubiquitin-conjugating enzyme UBE2O regulates cellular clock function by promoting the degradation of the transcription factor BMAL1. J Biol Chem 293, 11296–11309 (2018). [PubMed: 29871923]
9. Vila IK et al. A UBE2O-AMPKα2 Axis that Promotes Tumor Initiation and Progression Offers Opportunities for Therapy. Cancer Cell 31, 208–224 (2017). [PubMed: 28162974]
10. Huang Y et al. UBE2O targets Mxi1 for ubiquitination and degradation to promote lung cancer progression and radioresistance. Cell Death Differ 28, 671–684 (2021). [PubMed: 32901121]
11. Liu X et al. UBE2O promotes the proliferation, EMT and stemness properties of breast cancer cells through the UBE2O/AMPKα2/mTORC1-MYC positive feedback loop. Cell Death Dis 11, 10 (2020). [PubMed: 31907353]
12. Faust TB et al. The HIV-1 Tat protein recruits a ubiquitin ligase to reorganize the 7SK snRNP for transcriptional activation. Elife 7, e31879 (2018). [PubMed: 29845934]
13. Bagger FO, Kinalis S & Rapin N BloodSpot: a database of healthy and malignant haematopoiesis updated with purified and single cell mRNA sequencing profiles. Nucleic Acids Res 47, D881–D885 (2019). [PubMed: 30395307]
14. Novershtern N et al. Densely Interconnected Transcriptional Circuits Control Cell States in Human Hematopoiesis. Cell 144, 296–309 (2011). [PubMed: 21241896]
15. Wefes I et al. Induction of ubiquitin-conjugating enzymes during terminal erythroid differentiation. Proc Natl Acad Sci 92, 4982–4986 (1995). [PubMed: 7761435]

16. Brown A, Baird MR, Yip MC, Murray J & Shao S Structures of translationally inactive mammalian ribosomes. Elife 7, e40486 (2018). [PubMed: 30355441]
17. Husnjak K & Dikic I Ubiquitin-Binding Proteins: Decoders of Ubiquitin-Mediated Cellular Functions. Annu Rev Biochem 81, 291–322 (2012). [PubMed: 22482907]
18. Huang Q, Qin D, Pei D, Vermeulen M & Zhang X UBE2O and USP7 co-regulate RECQL4 ubiquitinylation and homologous recombination-mediated DNA repair. FASEB J 36, e22112 (2022). [PubMed: 34921745]
19. Zlatanova J, Seebart C & Tomschik M Nap1: taking a closer look at a juggler protein of extraordinary skills. FASEB J 21, 1294–1310 (2007). [PubMed: 17317729]
20. Park Y-J & Luger K Structure and function of nucleosome assembly proteins. Biochem Cell Biol 84, 549–549 (2006). [PubMed: 16936827]
21. Rodriguez P et al. Functional Characterization of Human Nucleosome Assembly Protein-2 (NAP1L4) Suggests a Role as a Histone Chaperone. Genomics 44, 253–265 (1997). [PubMed: 9325046]
22. Attia M et al. Interaction between Nucleosome Assembly Protein 1-like Family Members. J Mol Biol 407, 647–660 (2011). [PubMed: 21333655]
23. Rössler I et al. Tsr4 and Nap1, two novel members of the ribosomal protein chaperOME. Nucleic Acids Res 47, 6984–7002 (2019). [PubMed: 31062022]
24. Warren C & Shechter D Fly Fishing for Histones: Catch and Release by Histone Chaperone Intrinsically Disordered Regions and Acidic Stretches. J Mol Biol 429, 2401–2426 (2017). [PubMed: 28610839]
25. Michelle C, Vourc'h P, Mignon L & Andres CR What Was the Set of Ubiquitin and Ubiquitin-Like Conjugating Enzymes in the Eukaryote Common Ancestor? J Mol Evol 68, 616–628 (2009). [PubMed: 19452197]
26. Bartke T, Pohl C, Pyrowolakis G & Jentsch S Dual Role of BRUCE as an Antiapoptotic IAP and a Chimeric E2/E3 Ubiquitin Ligase. Mol Cell 14, 801–811 (2004). [PubMed: 15200957]
27. Sheng Y et al. A Human Ubiquitin Conjugating Enzyme (E2)-HECT E3 Ligase Structure-function Screen. Mol Cell Proteomics 11, 329–341 (2012). [PubMed: 22496338]
28. Plechanovová A, Jaffray E, Tatham MH, Naismith JH & Hay RT Structure of a RING E3 ligase and ubiquitin-loaded E2 primed for catalysis. Nature 489, 115–120 (2012). [PubMed: 22842904]
29. Roldan JLO et al. Distinct Ubiquitin Binding Modes Exhibited by SH3 Domains: Molecular Determinants and Functional Implications. Plos One 8, e73018 (2013). [PubMed: 24039852]
30. Stamenova SD et al. Ubiquitin Binds to and Regulates a Subset of SH3 Domains. Mol Cell 25, 273–284 (2007). [PubMed: 17244534]
31. Elliott PR et al. Regulation of CYLD activity and specificity by phosphorylation and ubiquitin-binding CAP-Gly domains. Cell Reports 37, 109777 (2021). [PubMed: 34610306]
32. Juszkiewicz S & Hegde RS Quality Control of Orphaned Proteins. Mol Cell 71, 443–457 (2018). [PubMed: 30075143]

Methods References

33. Labun K et al. CHOPCHOP v3: expanding the CRISPR web toolbox beyond genome editing. Nucleic Acids Res 47, W171–W174 (2019). [PubMed: 31106371]
34. Ran FA et al. Genome engineering using the CRISPR-Cas9 system. Nat Protocols 8, 2281–2308 (2013). [PubMed: 24157548]
35. Shimizu Y & Ueda T PURE technology. Methods Mol Biol 607, 11–21 (2010). [PubMed: 20204844]
36. Feng Q & Shao S In vitro reconstitution of translational arrest pathways. Methods 137, 20–36 (2018). [PubMed: 29277545]
37. Punjani A, Rubinstein JL, Fleet DJ & Brubaker MA cryoSPARC: algorithms for rapid unsupervised cryo-EM structure determination. Nat Methods 14, 290–296 (2017). [PubMed: 28165473]

38. Zivanov J et al. New tools for automated high-resolution cryo-EM structure determination in RELION-3. Elife 7, e42166 (2018). [PubMed: 30412051]
39. Sanchez-Garcia R et al. DeepEMhancer: a deep learning solution for cryo-EM volume post-processing. Commun Biol 4, 874 (2021). [PubMed: 34267316]
40. Varadi M et al. AlphaFold Protein Structure Database: massively expanding the structural coverage of protein-sequence space with high-accuracy models. Nucleic Acids Res 50, D439–D444 (2022). [PubMed: 34791371]
41. Pettersen EF et al. UCSF Chimera: A visualization system for exploratory research and analysis. J Comput Chem 25, 1605–1612 (2004). [PubMed: 15264254]
42. Emsley P, Lohkamp B, Scott WG & Cowtan K Features and development of Coot. Acta Crystallogr D 66, 486–501 (2010). [PubMed: 20383002]
43. Adams PD et al. PHENIX: a comprehensive Python-based system for macromolecular structure solution. Acta Crystallogr D 66, 213–221 (2010). [PubMed: 20124702]
44. Evans R et al. Protein complex prediction with AlphaFold-Multimer. Biorxiv 2021.10.04.463034 (2021) doi:10.1101/2021.10.04.463034.
45. Pettersen EF et al. UCSF ChimeraX: Structure visualization for researchers, educators, and developers. Protein Sci 30, 70–82 (2021). [PubMed: 32881101]
46. Croll TI ISOLDE: a physically realistic environment for model building into low-resolution electron-density maps. Acta Crystallogr D 74, 519–530 (2018).
47. Mirdita M et al. ColabFold: Making protein folding accessible to all. Nat Methods (2022). 10.1038/s41592-022-01488-1
48. Chen VB et al. MolProbity: all-atom structure validation for macromolecular crystallography. Acta Crystallogr D 66, 12–21 (2010). [PubMed: 20057044]
49. Barad BA et al. EMRinger: side chain–directed model and map validation for 3D cryo-electron microscopy. Nat Methods 12, 943–946 (2015). [PubMed: 26280328]
50. The PyMOL Molecular Graphics System, Version 2.4 Schrödinger, LLC.
51. Dong R, Pan S, Peng Z, Zhang Y & Yang J mTM-align: a server for fast protein structure database search and multiple protein structure alignment. Nucleic Acids Res 46, W380–W386 (2018). [PubMed: 29788129]
52. Madeira F et al. The EMBL-EBI search and sequence analysis tools APIs in 2019. Nucleic Acids Res 47, W636–W641 (2019). [PubMed: 30976793]
53. Larkin MA et al. Clustal W and Clustal X version 2.0. Bioinformatics 23, 2947–2948 (2007). [PubMed: 17846036]
54. Robert X & Gouet P Deciphering key features in protein structures with the new ENDscript server. Nucleic Acids Res 42, W320–W324 (2014). [PubMed: 24753421]
55. Ashkenazy H et al. ConSurf 2016: an improved methodology to estimate and visualize evolutionary conservation in macromolecules. Nucleic Acids Res 44, W344–W350 (2016). [PubMed: 27166375]
56. Rice P, Longden I & Bleasby A EMBOSS: The European Molecular Biology Open Software Suite. Trends Genet 16, 276–277 (2000). [PubMed: 10827456]
57. Morin A et al. Collaboration gets the most out of software. Elife 2, e01456 (2013). [PubMed: 24040512]

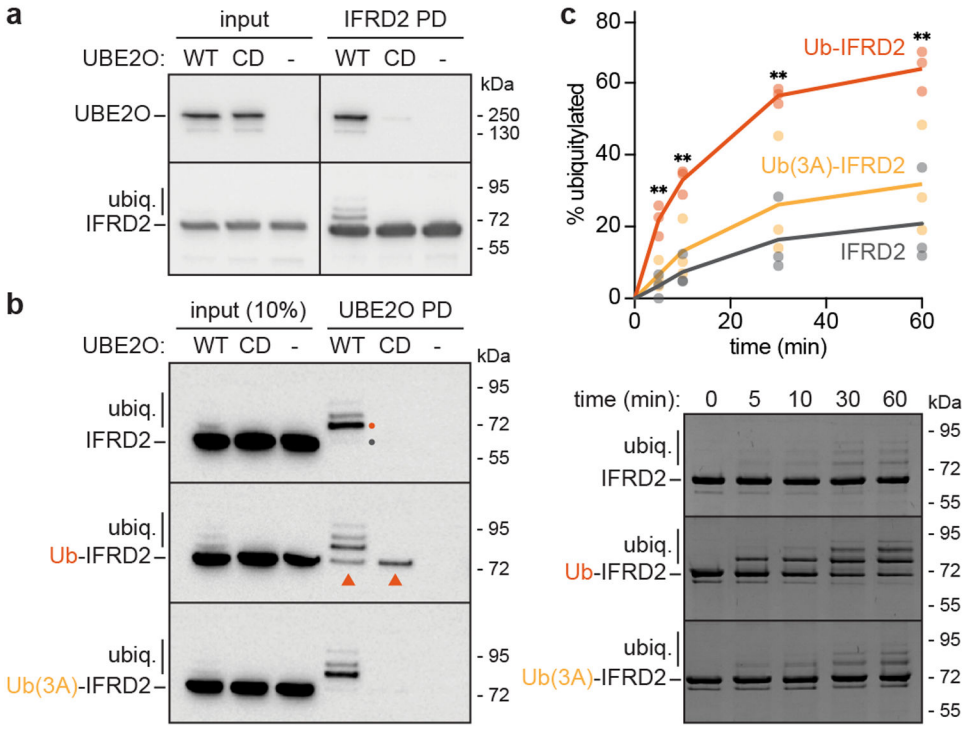

Fig. 1 | UBE2O preferentially binds and modifies ubiquitin-conjugated clients.

a, SDS-PAGE and immunoblotting of input and pulldown (PD) samples of FLAG-tagged IFRD2 co-expressed with wildtype (WT) or catalytically dead (CD) Strep-tagged UBE2O, or a transfection control (−), in HEK293T cells reveal a specific interaction between IFRD2 and WT but not CD UBE2O, representative of 3 replicates. ubiq., ubiquitylated IFRD2. **b,** UBE2O PD with unmodified IFRD2 (top) or with IFRD2 fused to G76V (Ub-IFRD2) or L8A/I44A/V70A/G76V ubiquitin (Ub(3A)-IFRD2) in UBE2O knockout HEK293T cells, representative of 3 replicates. Gray dot, unmodified IFRD2; orange dot, mono-ubiquitylated IFRD2; orange triangles, Ub-IFRD2 that pulls down with UBE2O. **c,** *In vitro* ubiquitylation timecourses of 2 μM of the indicated IFRD2 variant with 500 nM UBE2O, 75 nM E1, 10 μM ubiquitin, and an energy regenerating system. The average (line) percentage of ubiquitylated IFRD2 variant for 3 replicates (dots) is plotted versus reaction time (top). **, $p<0.01$ ($p=0.0043$ at 5 min, $p=0.0014$ at 15 min, $p=0.0028$ at 30 min, $p=0.0071$ at 60 min), unpaired two-tailed t-test between Ub-IFRD2 and IFRD2. SDS-PAGE and Coomassie staining of one replicate is shown below.

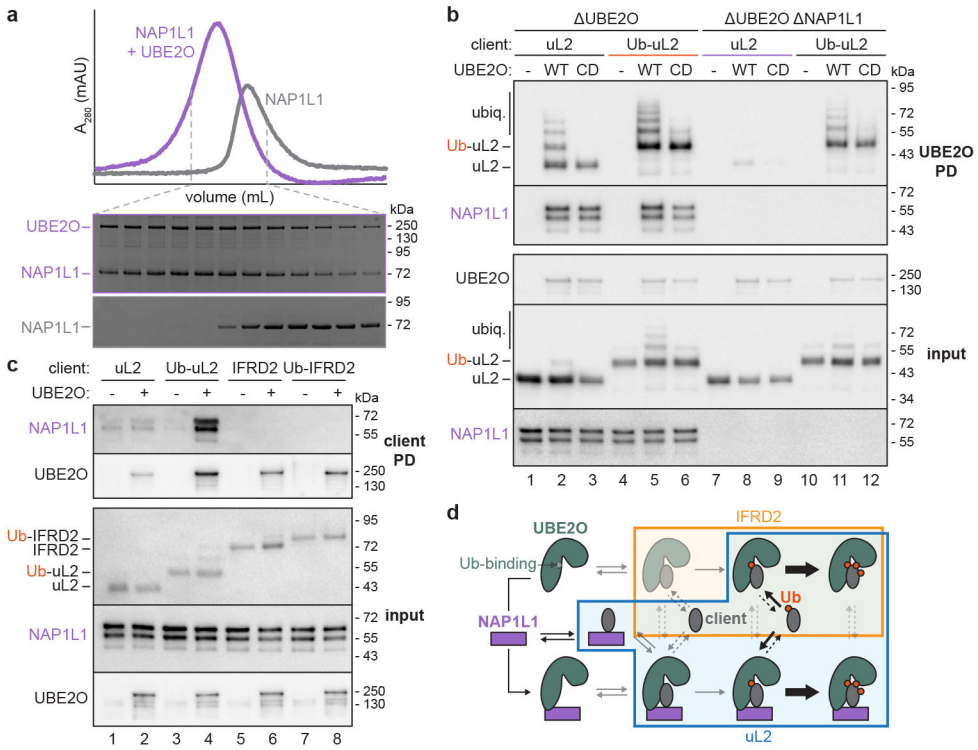

Fig. 2 | NAP1L1 is a UBE2O cofactor that regulates client selection.

a, Size exclusion chromatography trace (top) and SDS-PAGE and Coomassie staining (bottom) of purified NAP1L1 without (gray) or with (purple) UBE2O, representative of 2 replicates. **b,** Pulldowns (PD) of wildtype (WT) or catalytically dead (CD) Strep-tagged UBE2O co-expressed with the large ribosomal subunit protein uL2 without or with a ubiquitin fusion (Ub-uL2) in UBE2O knockout (ΔUBE2O) or UBE2O/NAP1L1 double-knockout (ΔUBE2O ΔNAP1L1) cells, representative of 2 replicates. **c,** PD of the indicated FLAG-tagged client expressed in ΔUBE2O cells without or with Strep-tagged UBE2O to detect endogenous NAP1L1 (purple) association, representative of 3 replicates. **d,** Model for UBE2O client selection mediated by an unannotated ubiquitin (Ub)-binding site and NAP1L1 as substrate adaptors. Opaque complexes are detected biochemically in our study. Outlined boxes indicate complexes observed with IFRD2 (light orange) or uL2 (blue).

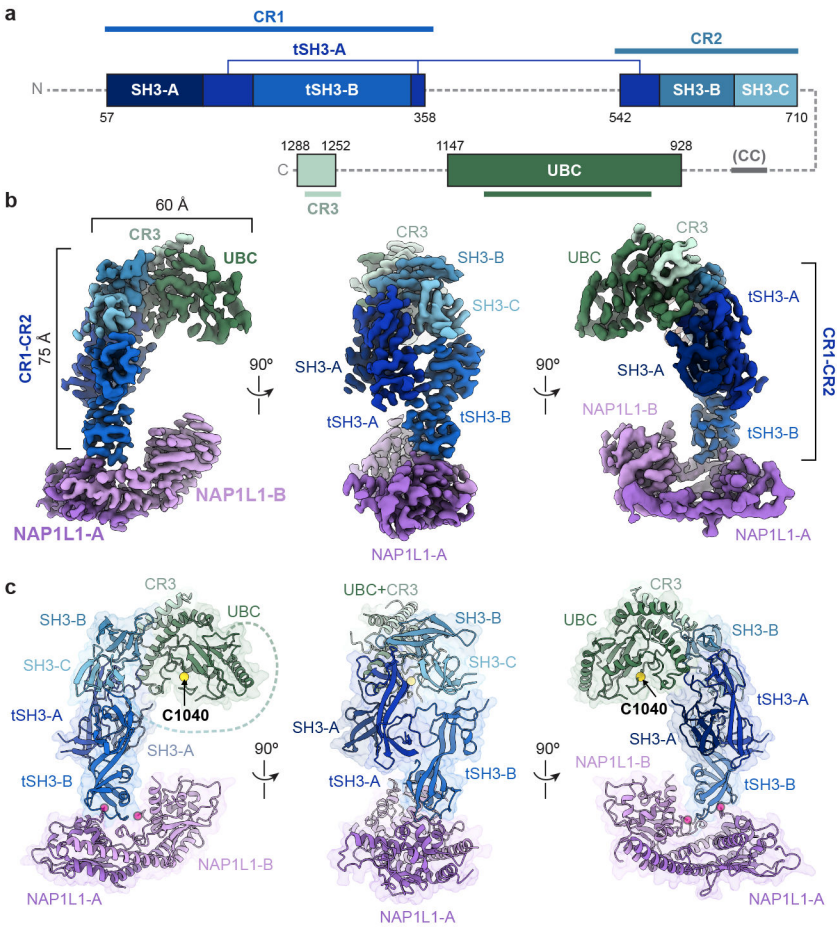

Fig. 3 |. Cryo-EM structure of UBE2O in complex with NAP1L1.

a, Linear domain organization of UBE2O. SH3-like domains (SH3-A, SH3-B, SH3-C), tandem SH3-like domains (tSH3-A, tSH3-B), the UBC domain, and CR3 visualized in cryo-EM structures are indicated. CR1, CR2, and CR3 are conserved regions. Colored lines denote previously annotated sequences for the indicated region or domain. CC, a putative coiled-coil not visualized by cryo-EM. Other unmodeled regions are indicated by dotted line. **b,** Cryo-EM map and **c,** model of UBE2O in complex with NAP1L1. The position of the catalytic cysteine (C1040; yellow sphere) and the C-terminal ends of NAP1L1 subunits (transparent magenta dots) are indicated. Blue/green dotted line indicates unresolved residues between tSH3-C and the UBC domain. The β5-β6 hairpin loop of NAP1L1 is not shown due to masking.

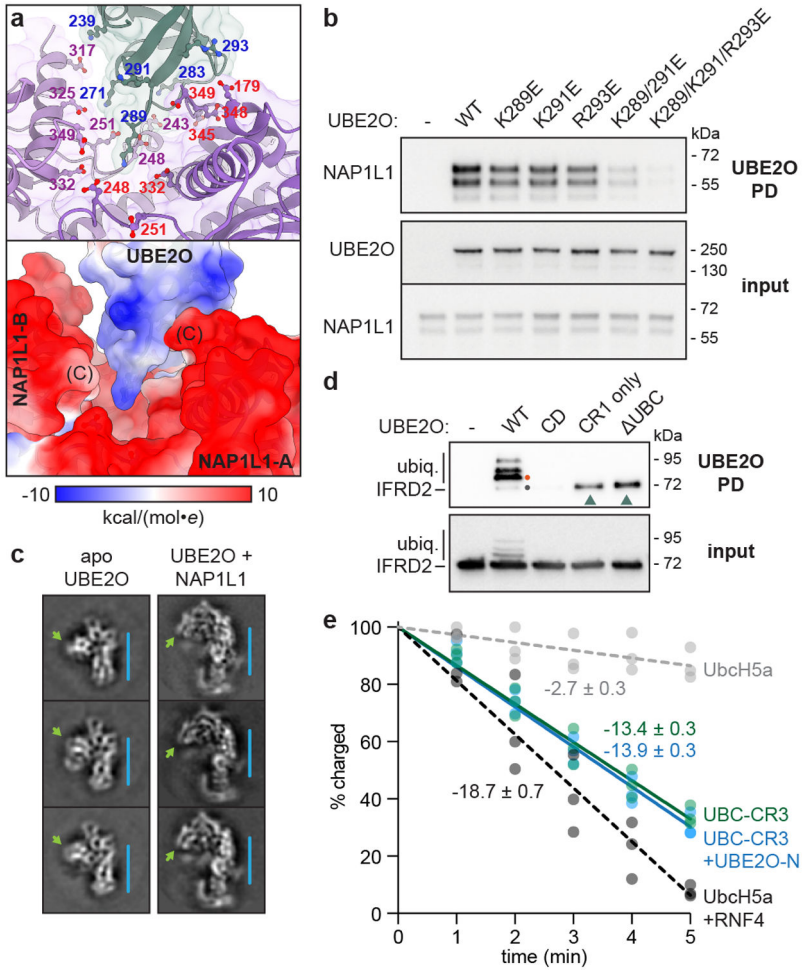

Fig. 4 |. Inter- and intra-molecular regulation of UBE2O activity.

a, The UBE2O-NAP1L1 interaction site showing positions (top) of basic residues in UBE2O tSH3-B (blue) and acidic residues in NAP1L1-A (red) or NAP1L1-B (purple), or colored by electrostatic potential with the C-terminal end of each NAP1L1 subunit indicated (bottom). **b,** Pulldowns (PD) of the indicated UBE2O variants to detect interaction with endogenous NAP1L1, representative of 2 replicates. **c,** 2D class averages of apo UBE2O and subtracted particles of UBE2O in complex with NAP1L1. The axis of CR1-CR2 (blue line, 60 Å) and relative position of the rest of UBE2O (green arrow) are indicated. **d,** PD of the indicated UBE2O variants reveal that the UBC domain autoinhibits client binding, representative of 2 replicates. CD, catalytically dead; CR1 only, the isolated CR1 region of UBE2O (residues 1-450); ΔUBC, UBE2O lacking the UBC domain (residues 944-1113); ubiq., ubiquitylated IFRD2; gray dot, unmodified IFRD2; orange dot, monoubiquitylated IFRD2. Teal arrowheads denote unmodified IFRD2 associated with CR1 and ΔUBC UBE2O. **e,** Timecourse of ubiquitin discharge from UBE2O UBC-CR3 without (blue) or with (green) UBE2O-N, or from UbcH5a without (gray) or with (black) the E3 RNF4. The percent of ubiquitin-charged E2 relative to t=0 min was quantified for three independent replicates, and a linear regression was applied to calculate the indicated discharge rate (% discharged per min).

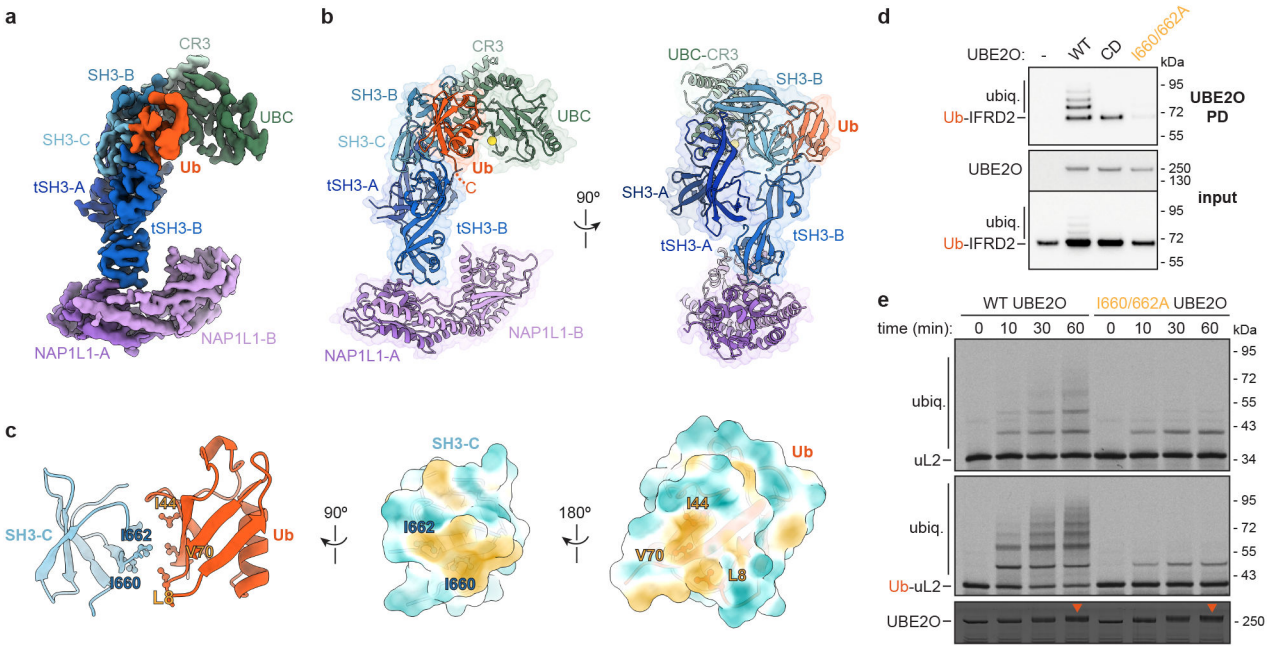

Fig. 5 | Ubiquitin makes a distinct interaction with an SH3-like domain of UBE2O.

a, Cryo-EM map and **b,** model of UBE2O-NAP1L1 bound to ubiquitin-fused uL2. The C-terminal end of ubiquitin (Ub; orange) is indicated by the orange dotted line. Yellow sphere denotes position of catalytic C1040. **c,** Interaction between hydrophobic patches on ubiquitin (L8/I44/V70) and on SH3-C of UBE2O. **d,** Pulldowns (PD) of wildtype (WT), catalytically dead (CD), or I660A/I662A Strep-tagged UBE2O co-expressed with FLAG-tagged ubiquitin-fused IFRD2 (Ub-IFRD2), representative of 2 replicates. ubiq., ubiquitylated Ub-IFRD2. **e,** *In vitro* ubiquitylation timecourses of radiolabeled uL2 (top) or ubiquitin-fused uL2 (Ub-uL2) (middle) with WT or I660A/I662A UBE2O, representative of 2 replicates. Coomassie staining showing UBE2O autoubiquitylation (orange arrowheads) is below.

Table 1.

Cryo-EM data collection, refinement and validation statistics

	UBE2O-NAP1L1 (EMDB-26614) (PDB 7UN6)	UBE2O-NAP1L1 with Ub (EMDB-26612) (PDB 7UN3)	UBE2O with Ub (focused) (EMDB-26615)
Data collection and processing			
Magnification	105,000	105,000	105,000
Voltage (kV)	300	300	300
Electron exposure (e–/Å^2)	57.4	59.6	59.6
Defocus range (μm)	−1.4 to −2.5	−1.4 to −2.5	−1.4 to −2.5
Pixel size (Å)	0.825	0.825	0.825
Symmetry imposed	C1	C1	C1
Initial particle images (no.)	4,138,230	3,677,176	3,677,176
Final particle images (no.)	447,881	201,743	639,300
Map resolution (Å)	3.3	3.5	3.5
FSC threshold	0.143	0.143	0.143
Map resolution range (Å)	3.1-4.9	3.4-5.1	3.2-4.5
Refinement			
Initial model used (PDB code)	AlphaFold Q9C0C9, P55209	UBE2O-NAP1L1, ColabFold	
Model resolution (Å)	4.1	4.1	
FSC threshold	0.5	0.5	
Model resolution range (Å)	4.1-30.2	4.1-29.5	
Map sharpening *B* factor (Å^2)	−141.0	−128.7	
Model composition	9,042	9,243	
Non-hydrogen atoms	9,042	9,243	
Protein residues	1,118	1,164	
Ligands	0	0	
B factors (Å^2)			
Protein	86.9	105.8	
Ligand			
R.m.s. deviations			
Bond lengths (Å)	0.005	0.004	
Bond angles (°)	0.980	0.982	
Validation			
MolProbity score	1.91	2.00	
Clashscore	11.10	13.26	
Poor rotamers (%)	0	0	
Ramachandran plot			
Favored (%)	95.0	94.7	
Allowed (%)	5.0	5.3	
Disallowed (%)	0	0	